Recent CEDRE Applications

**D. Scherrer, F. Chedevergne,
P. Grenard, J. Troyes, A. Murrone,
E. Montreuil, F. Vuillot,
N. Lupoglazoff, M. Huet,
B. Sainte-Rose, P. Thorigny,
N. Bertier, J.M. Lamet,
T. Le Pichon, E. Radenac, A. Nicole,
L. Matuszewski, M. Errera**

(Onera)

E-mail: : dominique.scherrer@onera.fr

A selection of recent CEDRE applications in the aerospace field are presented to illustrate various functionalities of the code. These applications have been selected to cover a wide application field in aerodynamics, aerothermodynamics and combustion. Many of them are “multiphysics”, in the sense that they are based on the coupling of independent solvers for, respectively, gas flow, condensed phase transport, solid conduction, radiation, etc. Some of them include an external coupling to other codes. The presentation of each application includes the objectives of the computation, the methodology (modeling, numerics, grid, etc.) and some significant results.

Introduction

CEDRE is the code used for nearly all energetics applications at Onera today. Its main application domain concerns internal flows in aerospace engines, but it has also been successfully used in other fields, due to its generality and its multiphysics positioning. CEDRE is based on the coupling of independent solvers for the gas flow (CHARME), a dispersed condensed phase (SPARTE in lagrangian formulation, SPIREE in eulerian formulation), solid conduction (ACACIA), stochastic gaseous particles (PEUL), radiation (REA with the DOM method, ASTRE with the Monte-Carlo method). A short description of the code and its solvers can be found in [43] and more detailed information on the methods and models can be found in other papers of the same Aerospace Lab issue [2][12][14][15][18][36][55]. In order to illustrate various functionalities of the code, some recent applications in the aerospace field are presented in this paper. The selected applications are listed hereafter with their general characteristics: RANS or LES, scientific field, specific modeling (if the case arises), solver(s).

- Aerothermodynamics of turbine blades: RANS, aerothermics, SIBLE wall function, CHARME
- Conjugate Heat Transfer applied to an effusion cooling system: RANS, fluid/structure aerothermics, MSD (CHARME’s predecessor) + external coupling
- Film-cooling of a dump combustor: RANS, fluid/structure aerothermics, reactive, CHARME
- Hypersonic vehicle separation: RANS, hypersonic aerodynamics, CHARME
- Rocket engine ignition blast wave: LES, aeroacoustics, equivalent gas two-phase flow, reactive, CHARME
- Jet noise prediction: LES, aeroacoustics, CHARME + external coupling
- Flow separation in an over expanded nozzle: RANS and DDES, reactive, CHARME
- Aircraft and helicopter icing: RANS, two-phase flow, SPIREE + external coupling
- Flow instabilities in a solid propellant motor: LES, flow instability, CHARME
- Combustion in a multipoint injection burner: RANS, diphasic, reactive, radiation, CHARME + SPARTE + ASTRE + PEUL
- Reacting flow in a research ramjet combustor: RANS&LES, reactive, CHARME
- Combustion in MASCOTTE cryogenic burner: RANS, sub/supercritical fluids, reactive, CHARME + SPARTE

Aerothermodynamics of turbine blades

Introduction

Due to limitations of computer resources in conception processes, the development of efficient methods for internal blade cooling system simulation on coarse grids is a necessity for industrials. Onera has thus been invested in the implementation and development of such methods in its energetics code CEDRE. The main objective is to provide a set of numerical tools allowing the simulation of complex configurations with reasonable accuracy. In the aerothermodynamics context, particular attention has been paid to EARSM (Explicit Algebraic Reynolds Stress Model) turbulence models [62] for their ability to simulate rotating flows. In the same time, Onera has developed an advanced wall function, SIBLE (Simple Integrated Boundary Layer

Equations) [10], able to take account for pressure gradients. The goal of the present simulations is the validation of these two models in a simplified but representative configuration.

Configuration

The BATHIRE rig [49] is a recent facility installed at the Palaiseau Onera center, to study rotating internal blade cooling systems. The U-bend test section reproducing a part of a cooling passage is equipped with optical and thermal access so that PIV and infrared measurements can be performed. Consequently, on the same rig, we have access to the flow structure and to heat exchanges on a heated wall. This wall can be equipped with ribs but only the smooth configuration will be considered here. The geometry of the test channel consists of two parallel ducts connected with a constant height curved duct. The hydraulic diameter is kept roughly constant, equal to 50, along the rig. Based on this length, the Reynolds number is found to be equal to 25000. The Rossby number, characterizing the rotation effects, is fixed at 0.33 corresponding to a rotation rate of the rig equal to 500 rpm.

The inlet conditions are quite complex, due to the junction between the primary circuit on the rotating axis and the main channel, which induces a swirl. Reproducing this upstream condition is crucial to accurately simulate the flow and compare the results to the measurements. The retained configuration is presented in figure 1.

Computation methodology

The computational domain has been meshed using CENTAUR, resulting in a 3D unstructured grid with 3 prism layers at the walls. Finally, only 690,000 cells are used to discretize the whole domain. This deliberate limitation was made to stay within the specification bounds, i.e. performing simulations on coarse grids.

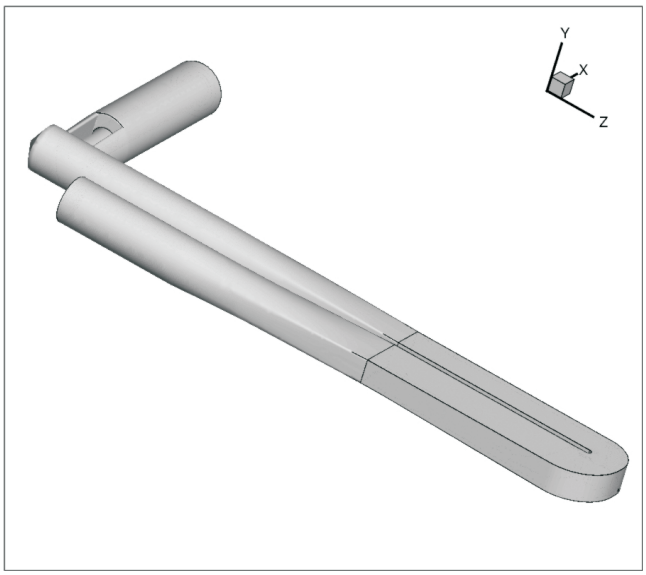

Figure 1 - Global view of the computational domain

The EARSM/EAHFM models, based on the work of Wallin and Johansson [62] and Wikström [63], have been used. To complete the modeling, the SIBLE wall function [10] has been activated. This original wall model locally solves a set of boundary layer equations and thus provides a good evaluation of the friction and heat exchange coefficients, compared to a conventional wall function.

Computation results

PIV measurements

First, we focus on the PIV measurements and compare them to the simulation results. Globally speaking, it appears that the flow is well reproduced by the CEDRE code, using the retained models. Figure 2 illustrates this good agreement: on this plane, one can clearly identify two separation zones, placed identically in both the measurements and the simulation. Other simulations using standard turbulence models, such as the k-ω SST of Menter, show that these models are unable to reproduce this particular phenomenon due to rotation. Good agreement must be tempered, because of a velocity deficit in the inlet plane of the U-bend. This deficit may be attributed to a bad description of the inlet swirl mentioned earlier. The grid, deliberately chosen to be coarse, may be responsible for the difference between simulation and experiments. However, the simulations clearly show the relevance of the chosen models, allowing a quite good description of the flow on a coarse mesh.

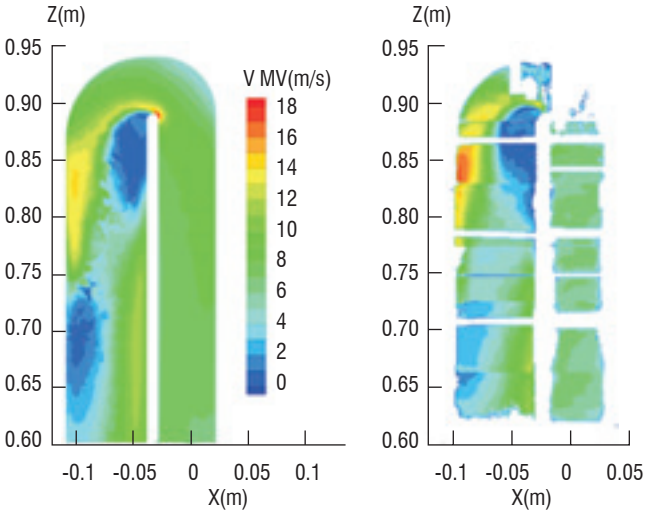

Figure 2 - Comparison between the computation (left) and the experiment (right) for the velocity magnitude

Heat exchange measurements

Heat exchanges are deduced from the wall temperature measurements provided by the thermal camera. An estimate of the heat flux imposed at the wall is gained a posteriori from a 2D thermal conduction solver. Unfortunately, up to now, the method is such that there are many uncertainties on the deduced heat flux, in particular because of the difficulty to estimate the losses by the back side of the rig, especially during rotation tests. Finally, the heat exchange coefficient is calculated thanks to the following formula :

$$h = \frac{\varphi}{T - T_{ref}}$$

The reference temperature T_{ref} is defined as a linear interpolation between the inlet and outlet sections of the test passage following the median curvilinear path.

Numerical results are obtained with an imposed constant heat flux on the heated wall, whereas other walls are assumed adiabatic, and the same process is applied to deduce the h field. Comparison between the computation and the experiment is given in figure 3.

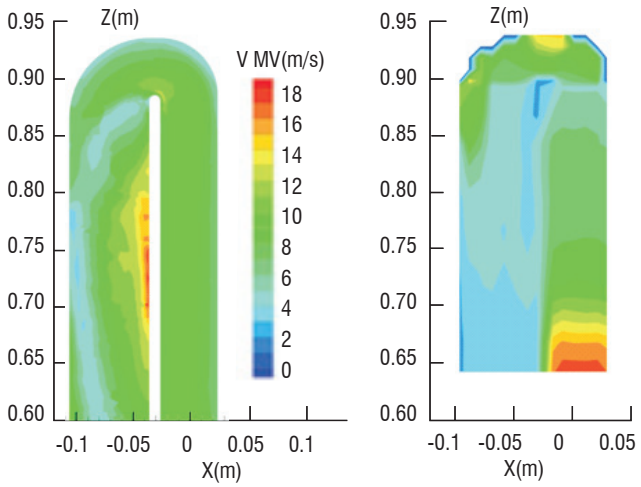

Figure 3 - Comparison between computation (left) and experiment (right) for the heat transfer coefficient h

The results look different, but the average values of h are roughly the same in both the calculation and the experiment. Future tests with a reconsidered heat system should bring answers to the remaining questions, such as the one concerning the CEDRE code validation. However, a reasonable confidence can be attributed to these calculations in regard to the thermal aspects, thanks to the good agreement obtained in the aerodynamic field.

Conclusion

Through this example, recent models implemented in the CEDRE code are shown to be able to capture the main effects encountered in the aerothermodynamics context of turbine blade cooling systems. The velocity field is quite well predicted, however some discrepancies remain concerning the thermal fields, possibly due to experimental uncertainties, for which the validation effort will be continued.

Conjugate Heat Transfer applied to an effusion cooling system

Introduction

The numerical test presented in this section provides a computational example of conjugate heat transfer analysis in a severe thermal case of an effusion cooling-system, in the context of a steady state problem. The basic approach used here is based on a coupled partitioned method, in which physical systems are spatially decomposed into partitions. The solution is separately advanced in time over each partition. Here it corresponds to the loose coupling of a finite-volume Navier-Stokes solver (MSD, CHARME's predecessor for structured grids), in the fluid domain and a finite-element heat conduction solver (a solver of the Zset-code) in the solid domain. The goal of this presentation is to prove that a predictive procedure may be efficient to capture the local behavior of mass and heat transfer in an effusion-cooling system.

Geometry of the effusion system

The cooling configuration in this study has been scaled from actual combustion geometries and contains the essential physics of an effusion-cooling system, except for the curvature. It would be unrealistic to take into account the full-coverage discrete hole film-cooling, since such a typical configuration may contain thousands of holes. As a consequence, a geometrically simple film cooling configuration has been chosen. It consists of 2 staggered rows of circular holes (elliptic in the xz-plane) with the same orientation angle θ. Figure 4 shows a top view of the physical domain with the 12 cooling holes and also a side view of one oblique hole through the combustion skin.

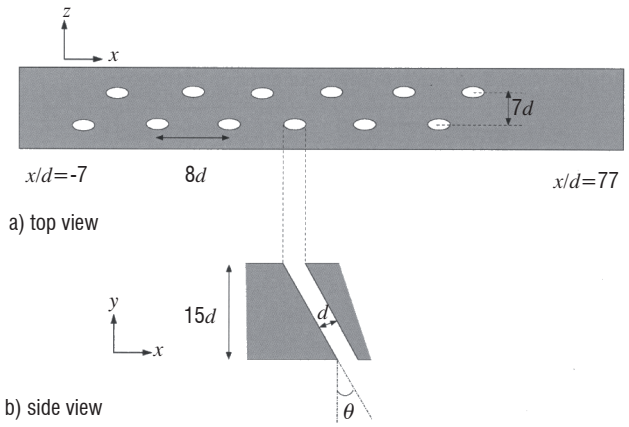

Figure 4 - Staggered arrangement of cooling holes

Geometric data relevant to the effusion cooling configuration are summarized in the following table:

hole diameter	injection angle	solid thickness	hole-to-hole spacing	solid length
0.27 mm (d)	45°	4 mm (15 d)	2.2 mm (8 d)	22 mm (84 d)

Computation methodology

The coupling procedure begins with an uncoupled fluid computation, assuming adiabatic surfaces. This first computation defines the initial conditions for the coupled thermal simulation. Then, the coupling algorithm consists of an unsteady time integration in the fluid, while a steady calculation is carried out in the solid [21]. Each domain is solved independently using the conditions produced by the other. At each interface separating the fluid and solid domains, we must ensure that both the temperature and the heat flux are identical in the steady state. Dirichlet conditions are imposed in the solid side, while Robin conditions are used in the fluid side. For more details, see [21] and [11]. A dynamic coupling strategy has been used here: each coupling step is automatically performed when the evolution of the fluid temperature near the coupled interface is significant. This procedure reduces the computing time significantly.

The velocity, the turbulence ratio and the total temperature of the cold mainstream are 20 $m.s^{-1}$, 2% and 600 K respectively. In the hot crossflow they are equal to 370 $m.s^{-1}$, 3% and 2200 K respectively. The Reynolds number in the hot gas flow is 2.10^6. Cooling air is injected at the blowing rate of 1.2 and the momentum flux ratio is 0.5 in the hot main stream. The solid thermal conductivity is 14 $W.m^{-1}.K^{-1}$ (steel). In this study, the flow equations are closed using the two equation k-l turbulence model with wall functions [27].

Computation results

Only the main features are presented here, more details can be found in [11] and [17]. The temperature contours are shown in figure 5. For clarification, they are plotted using two different scales, one in the solid, the other in the fluid. Several salient features may be observed. First, the formation and penetration of the effusion jets into the hot main stream is evident. It is also clear that the solid temperature pattern changes from hole to hole. Small zones of high temperature downstream in the film can also be seen. This can be partially explained by the existence of secondary flows.

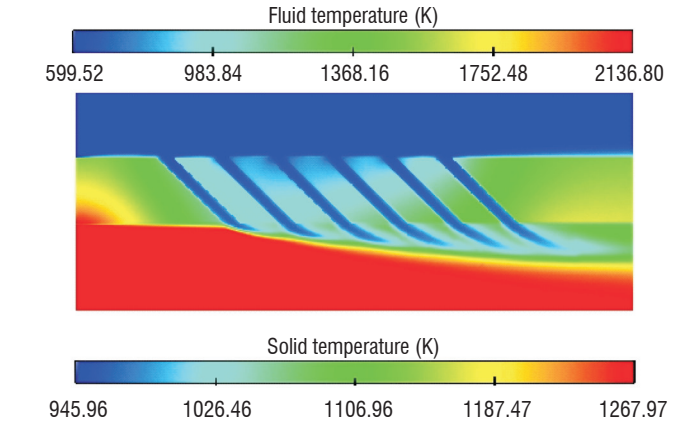

Figure 5 - Temperature field

Some streamlines are depicted in Figure 6, in an xy-plane cutting through the 1st row of holes. The incoming cooling flow separates at the sharp edge of the effusion holes and reattaches very rapidly. The main velocity in a hole is approximately 150 $m.s^{-1}$.

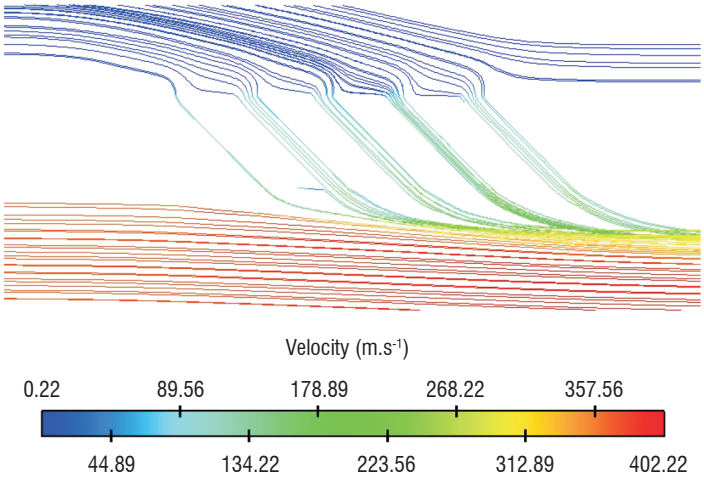

Figure 6 - Velocity streamlines

Figure 7 shows the velocity field at 4 selected yz-planes in the hot gas flow. The axial position of each plane is indicated in this series of plots. The velocity vectors are colored by the temperature magnitude. A double vortex structure has developed close to the wall, downstream of the effusion jets. The hot main stream is drawn into zones located in the middle of the two rows of holes, generating two counter-rotating vortices.

These structures allow the hot main stream to flow above the cooling jets. At increasing x/d positions, the secondary vortices become strengthened, resulting in a heat transfer enhancement, from the hot gas to the wall. This process reduces the effectiveness of the film cooling. However, it must be remembered that film cooling flows are complex and are characterized by complicated structures (kidney vortex, shear layer vortices, wake vortices, etc.) generally not well predicted by eddy viscosity models. As a consequence, a DNS or LES approach could lead to better numerical predictions. Nevertheless, this study has shown that a coupled approach can provide detailed insights into the underlying phenomena of the effusion cooling and allows different parameters to be evaluated under realistic conditions.

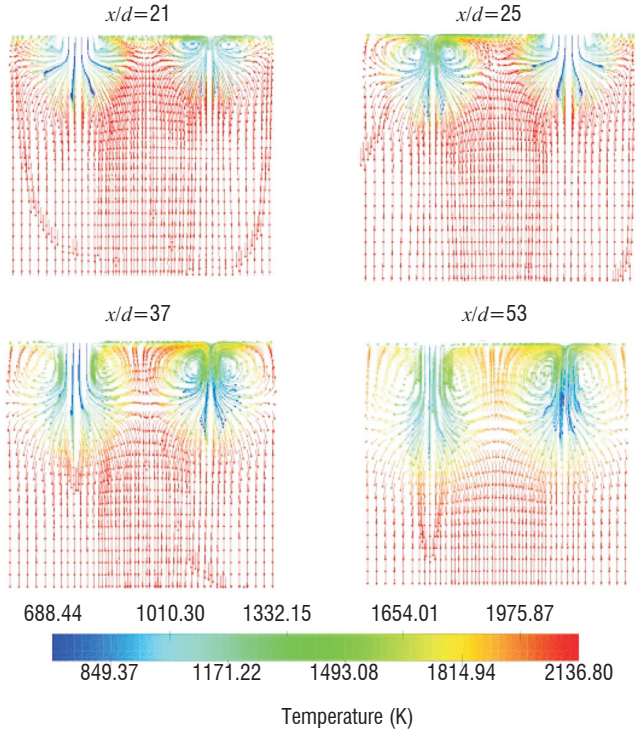

Figure 7 - Velocity vectors in xy-planes

Conclusion

Fluid/structure coupled computations for aerothermodynamics have shown their ability to provide detailed insights into the phenomena underlying the effusion cooling. Such computations have more recently been performed with CHARME for a gas and ACACIA for a solid (two CEDRE solvers) to quantify the effect of various parameters on the heat transfers and contribute to the improvement of the CEDRE perforated wall model (see the following section, “Film-cooling of a dump combustor”). The following step for these computations is the LES approach.

Film-cooling of a dump combustor

Introduction

In order to cool combustion chambers, an efficient method, known as film-cooling, consists in blowing “fresh” air through multiperforated walls. In the preceding section we have seen a coupled fluid/structure computation for a small wall fraction including only a few holes. Since in actual configurations the walls can be pierced by hundreds thousands of small (diameter less than 1 mm) holes, a meshing of all these holes is unthinkable and the heat and mass transfers inside the perforated walls must be modeled. A specific model was thus developed to compute the mass flow rate through the wall and the temperature and heat flux on both wall faces locally. The model

actually provides coupled boundary conditions for the flow on each side of the wall. After a short description of the model principle, we present a simulation of an experimental dump combustor cooled by this technique. The goal of this simulation is to show the operationality of the model and show its interest in the industrial design process.

Principle of the model

The perforated wall model must not be viewed as a boundary condition for CHARME (the CEDRE Navier-Stokes solver), but as a simple analytical one-dimensional solver for the perforated wall (solid + cooling fluid) between the two faces (figure 8). Its implementation in CEDRE includes an automatic coupling with CHARME on each face of the wall.

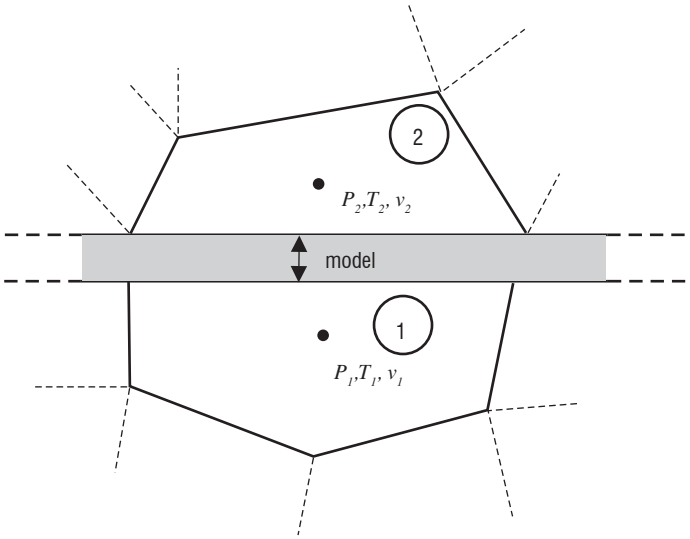

Figure 8 - Principle of the model (macroscopic point of view)

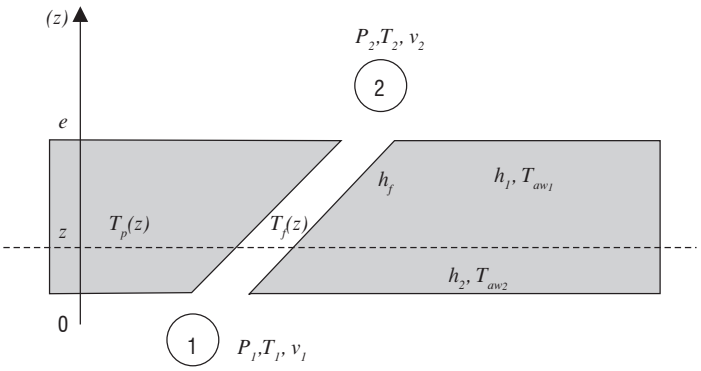

Figure 9 - Principle of the model (detailed solution)

The model is made of two independent parts, namely the aerodynamic part, which provides the mass flow rate, and the thermal part, which provides the temperatures and heat fluxes. The aerodynamic part computes the mass flow rate through the wall from a semi-empirical correlation depending on the geometry (wall thickness, hole diameter and angle, porosity) and on the pressure difference between the two faces. The thermal part is based on the analytical resolution of the coupled one-dimensional steady equation system for the cooling air temperature and the solid wall temperature, under a thermal equilibrium assumption (figure 9). Details of the equations and their solution will be the subject of another future publication.

Dump combustor configuration

This model was applied to a DUMP combustor for two operating conditions. The combustor geometry is nearly axi-symmetric except for the fuel injection system (see figure 10).

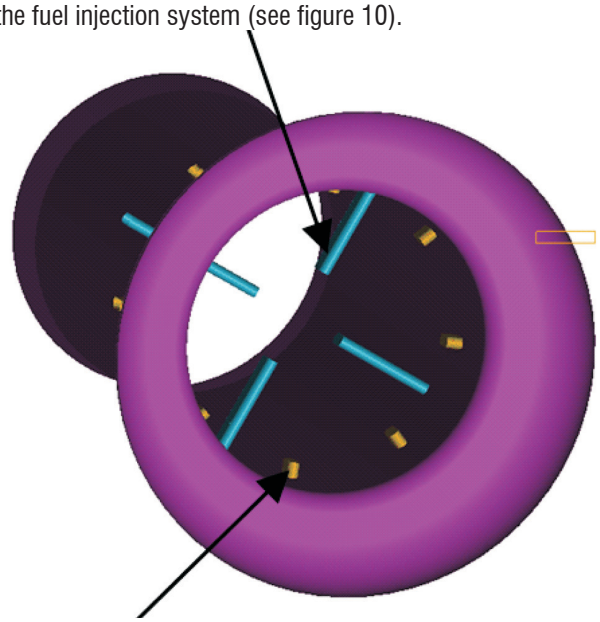

Figure 10 - Distribution of the injectors (main injectors in blue, pilot in orange)

Due to the symmetry planes, only ¼ of the geometry is computed: the computed geometry is represented in figure 11.

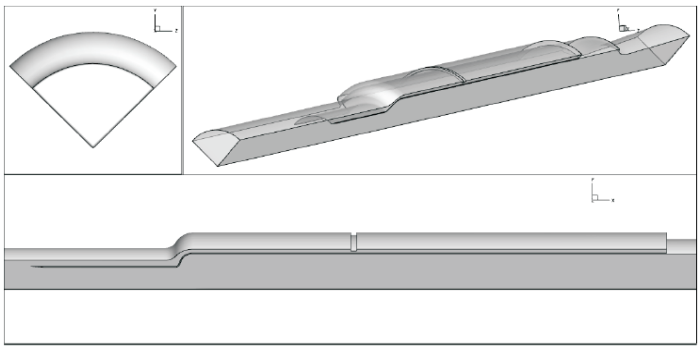

Figure 11 - Computed geometry

The multiperforated wall separating the cooling channel and the combustor is divided into three different sections with different porosity, hole orientation and hole diameter. At the interface between the first and the section, the cooling channel is partially closed over about 50% of its height, in order to increase the pressure difference in the first section, where the heat fluxes are assumed to be the highest. The main geometrical parameters are shown in figure 12.

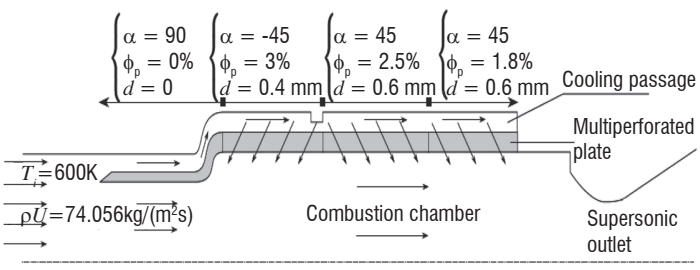

Figure 12 - Geometrical parameters of the cooling plate

Liquid kerosene is injected directly into the fluid at the position of the actual injectors (they are not meshed in our computation), as small droplets with a diameter of 15 μm and a temperature of 300 K.

Two operating points (presented in the table hereafter) have been computed.

Case	Air mass flow	Fluid temperature	Mixture ratio
Low Pressure	1.14 kg/s	606 K	0.6
High Pressure	7.1 kg/s	537 K	0.5

Computation methodology

The overall system is solved using a coupled CHARME-SPARTE methodology. SPARTE is used to compute the liquid droplets, while CHARME deals with gas aerodynamics and combustion. The turbulence model is the well-known k-ω SST and the combustion model is Eddy-Break-Up with $C_{EBU}=4$.

Experimental data consist in 6 temperature measurements on the cooling side of the wall. Although these points are not aligned in the experimental setup, they are all arranged behind the 4 main injectors. For symmetry reasons, we can expect them to behave almost as if they were aligned.

Computation results

The comparison between computed and measured wall temperature is presented in figure 13 for the low pressure case and in figure 14 for the high pressure case. For each case, both measurements and computation show two peaks in the temperature curves. The first peak is due to the combustion of the “pilot” kerosene and corresponds to the reattachment of the flow downstream of the section enlargement.

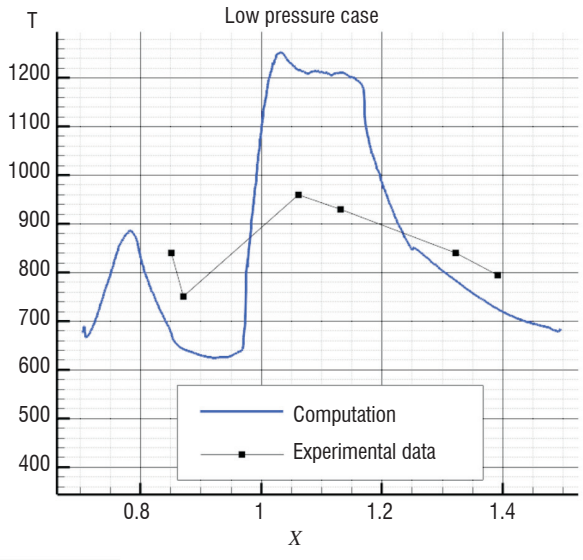

Figure 13 - Comparison between computed wall temperature and experimental data (low pressure case)

The second peak was more unexpected. In fact, as shown in figure 15, it is due to a too high pressure drop in the cooling channel at $x=0.95$, which corresponds to the position of the section restriction. The consequence is that the pressure difference between the cooling channel and the combustion chamber becomes very small, and even locally negative (i.e. some combustion gases are ingested into the cooling channel) so that the cooling is no more efficient in this region, which results in a high temperature peak.

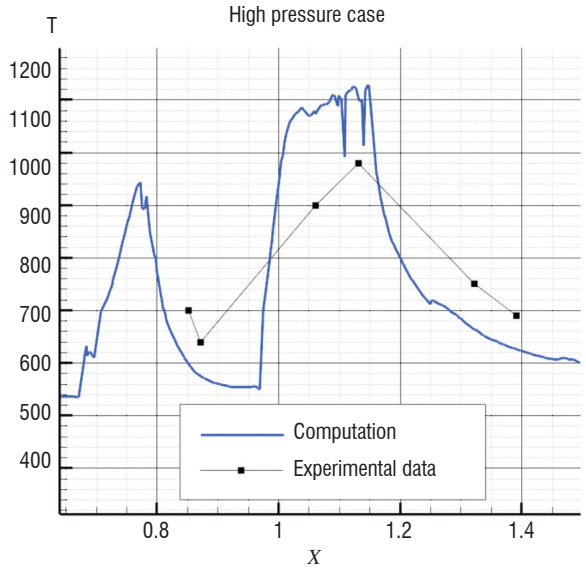

Figure 14 - Comparison between computed wall temperature and experimental data (high pressure case)

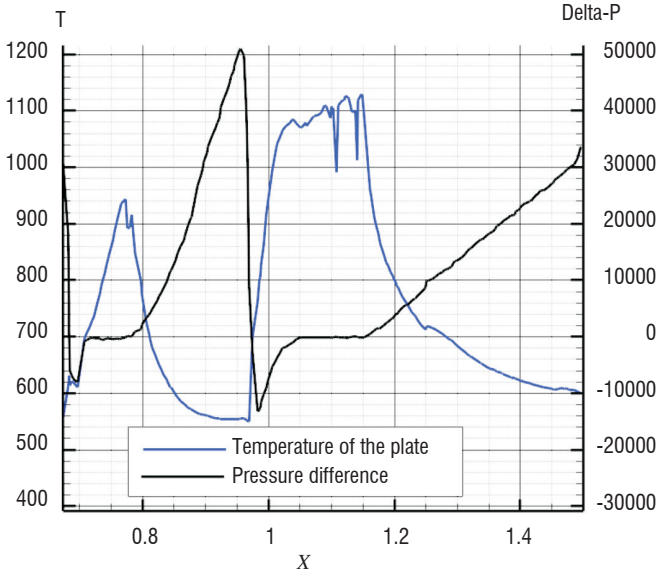

Figure 15 - Link between temperature evolution and pressure difference on the wall (high pressure case)

However, the wall temperature peak in regions where the pressure difference is vanishing seems to be overestimated by the computation. A possible explanation is the existence of small pressure fluctuations not captured by the RANS computation, which may help the fluid to move into the holes, therefore cooling the plate. The same phenomenon can be observed in the low pressure case. The combustion model, known to overestimate the gases temperature in the burner, is another possible explanation for these discrepancies.

Conclusion

A simplified multi-perforated wall model has been developed, implemented and tested to take into account multi-perforated walls in a global CFD computation. Even though wall temperature prediction is

perfectible, the model has been proven to be capable, at a negligible computational cost, of giving qualitatively good results and makes it possible to understand the effects of the cooling channel geometry on the temperature distribution on the wall. It can also be noted that wall temperature levels depend not only on the multi-perforated wall model, but also on several other models, such as the friction computation (turbulence model and wall law), the combustion model and the radiation for example. A validation based on simpler (without combustion) dedicated experiments will make it possible to improve the accuracy of wall temperature prediction.

Hypersonic vehicle separation

Introduction

The interest of high-speed air breathing propulsion has been identified for many years. Capability to sustain high altitude hypersonic cruise is particularly interesting in the scope of long-range missiles. Since January 2003, MBDA and Onera have been engaged in the LEA program [51][19][20], of which the most challenging issue is to show the capability to precisely assess the thrust-minus-drag balance of an experimental scramjet vehicle. Within the framework of the LEA program, Onera conducts CEDRE numerical simulations of the separation phase between the LEA vehicle and its booster.

The test flight sequence plans are for the experimental vehicle to be boosted up to the required flight tests conditions, after an air-drop from a Russian supersonic bomber. Once they are reached, LEA separates from its booster and starts its autonomous scramjet propelled flight. The separation between LEA and its booster will most likely be one of the most critical phases of the flight experiment. Thus, RANS computations were conducted to evaluate the aerodynamic interactions between LEA and the inter-stage of the booster during separation.

Since it was impossible to comprehensively characterize all the positions of LEA during the separation phase, only the most probable relative attitudes between the vehicle and its booster have been studied. Some of them are presented in figure 16.

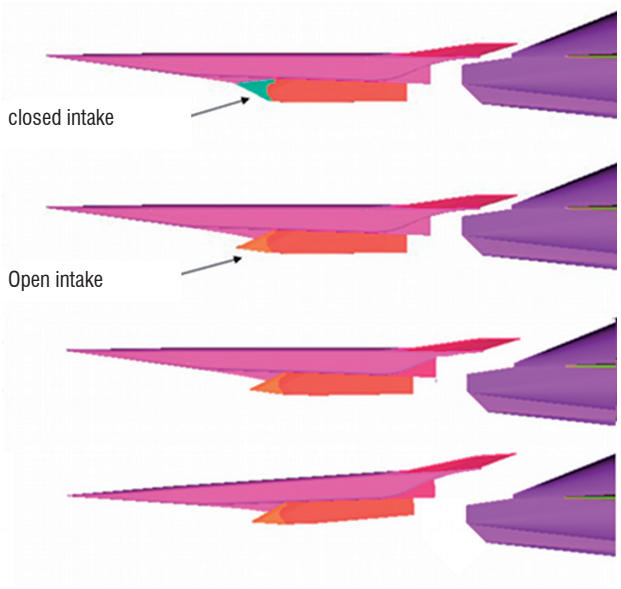

Figure 16 - Different relative separation positions studied

Computation methodology

The simulations were conducted at Mach 7.5, with CEDRE v3.2.2 on 3D unstructured half-configuration grids (12 M elements) (figure 17). The unstructured mesh allows the modeling for both vehicles of very complex shapes and mesh refinement in the interaction region.

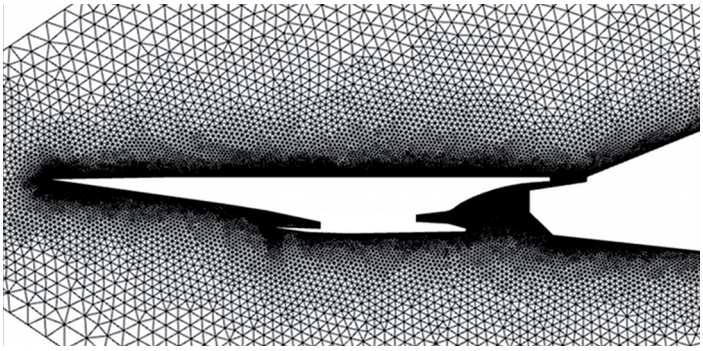

Figure 17 - Plane of symmetry of the grid used for separation computations

The RANS steady computations use the k-ω turbulent model with a low Reynolds approach (no wall law). The spatial resolution scheme is the Advection Upstream Splitting Method (AUSM+) with additional numerical dissipation activated : this flux scheme represents a good compromise between accuracy and robustness for supersonic flows. The one step implicit formulation with a local time step based on dU/dt is used as a time integration method. The calculations were carried out on 64 processors of an Altix ICE 8200 EX SGI supercomputer and each one took 10 hours to reach convergence after 5000 cycles.

Computation results

The computation results highlight an important flow interaction between the bow shock created by the inter-stage of the booster and the LEA nozzle boundary layer. This induces an important flow separation beginning at the maximum slope angle point of the upper part of the nozzle (figure 18). The flow separation disappears once the interaction shock is located downstream from the end of LEA's nozzle.

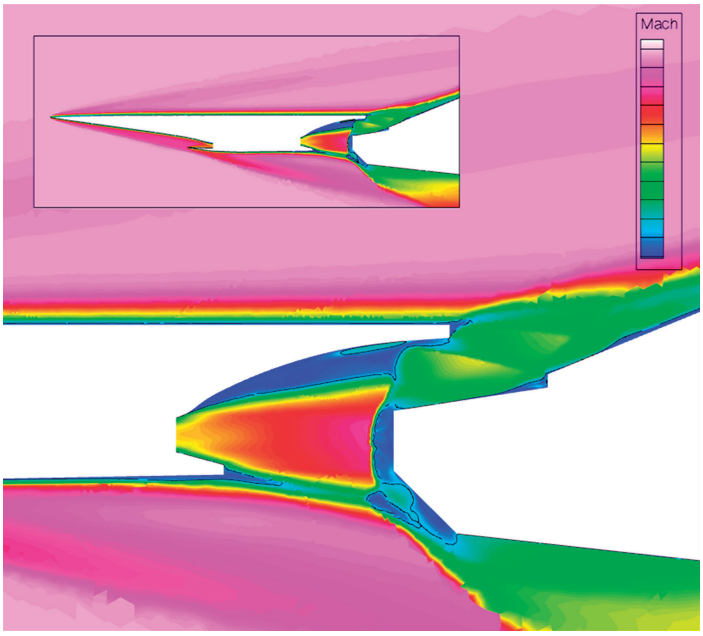

Figure 18 - Mach number in the symmetry plane (Intake opened)

When the intake is closed, figure 19 shows that the front part of the booster is in a kind of cavity flow. Then, no noticeable interaction is evidenced on the upper part of the nozzle compared to the LEA closed engine free flight computation. The free flight model could be considered unchanged in that particular case.

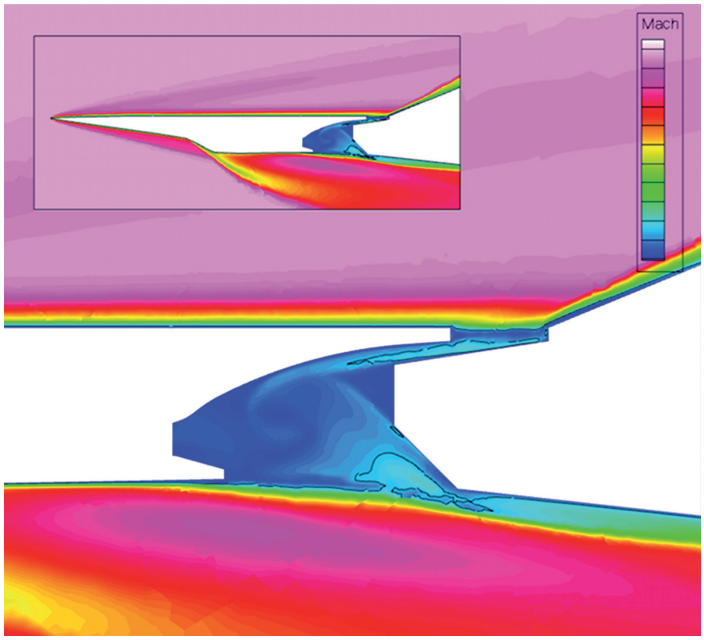

Figure 19 - Mach number in the symmetry plane (Intake closed)

Conclusion

Aerodynamic simulations of the separation of a hypersonic vehicle were successfully performed with CEDRE. In the next phase of the study, thanks to the general thermochemical model of the code, it will be possible to evaluate the effect of a high temperature real gas flow on the interaction. The high temperature could be due to high speed flow wall friction or to an early starting of the scramjet engine. A "moving bodies" functionality, currently being developed in the code, will allow to perform unsteady computations in the future.

Rocket engine ignition blast wave

Introduction

During a space vehicle launch, the rapid pressure build-up in the Solid Rocket Motor (SRM) chamber generates a strong overpressure wave at the nozzle exit, known as an Ignition OverPressure (IOP). One part is transported inside the flame trench to its exit, where it generates a second acoustic wave, the Duct OverPressure (DOP). These two low frequency waves may turn out to be dangerous, since they apply strong loads to the launch pad, the launcher or its payload. One of the main concerns of the CNES/Onera AEID program is to efficiently reduce these loads. Within this framework, experimental firings of scaled down models of Ariane 5 P230 SRM (known as LP10), were carried out at the Fauga Mauzac Onera center in various configurations [58]. Two of these are selected for the current study: a free horizontal jet (case I) with slightly aluminized propellant (5% in mass) and a realistic vertical firing with a flame trench (case II) with aluminum free propellant. In both cases, the nozzle is characterized by the ratio A_j/A_t=7.5625 between its exit area and its throat area, with an exit diameter D_j=70.34 mm. Pressure signals on far field and combustion chamber transducers were recorded during experiments.

The Onera CEDRE platform is used to perform numerical studies for these experiments. Various phenomena are modeled: the interaction of the acoustic waves with the environment (flame trench, ground, etc.), possible reactions between the reducing combustion products and the quenching with water of ambient air or combustion products. The inlet boundary is treated by imposing a total pressure fitting the experimental unsteady curve. The first 30 milliseconds are calculated with implicit time integration. The LES Smagorinsky sub grid model is activated.

Case I focuses exclusively on IOP: previous computations held in a 2D axisymmetric configuration yielded deceptive results regarding the amplitude and directivity [56]. Since the discrepancies were thought to be due to the 3D nature of the turbulence, 3D computations are carried out in case I. The aim of case II is to numerically characterize both IOP and DOP waves. Again, previous computations led to a quite accurate prediction of IOP and DOP, but a secondary DOP appeared, not observed during experiments [57]. The effect of the water supply in the flame trench is studied in case II. In both cases, the possible afterburning of combustion products with air is taken into account.

Free jet configuration (case I)

In the free jet configuration, the motor is fired horizontally, 1 meter above the ground. Transducers are located along a horizontal arc centered at the nozzle throat, with a 5 m radius and extending from 20 to 60° from the jet axis.

Computational Domain

The computational domain is a half-sphere centered on the nozzle throat, whose radius extends to 8 meters and truncated by the ground, as shown in Figure 20. It features the combustion chamber aft end, the nozzle and part of the motor structure.

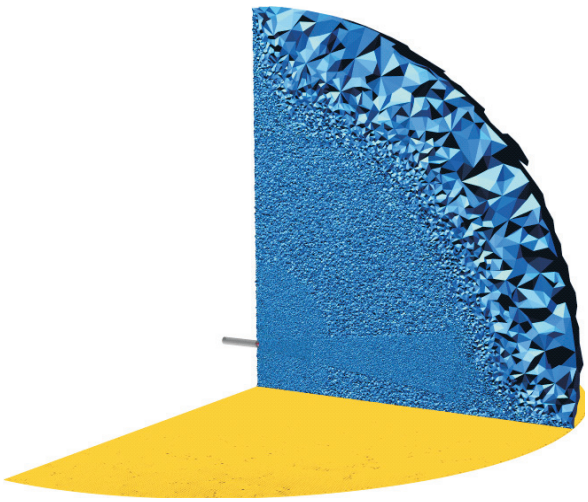

Figure 20 - Computational domain and grid

Grid

Particular attention must be paid to the size of cells propagating acoustic waves. Bogey and Bailly [5] showed that for low order space discretization schemes (typically 2, as used in this study), a minimum of 20 points must be found in the propagative direction in the consi-

dered wavelength (PPW), in order to ensure low dispersion and dissipation. The IOP wave front characteristic period can be estimated to $T=1$ ms, according to experimental data. The characteristic wavelength comes to $\lambda=c\times T=0.346$ m, where c is the sound speed in the propagative area (normal conditions of pressure and temperature). Thus, the maximum cell size in the direction of propagation is $\Delta=0.346/20=17.8$ mm. The generated cells being formed with an average number of 13 faces, they can easily be assimilated to spheres and the above criterion is to be applied to the cell diameter. In our domain, the resulting grid would yield far too many cells and a refinement procedure must be applied: cell size varies between 8 mm (at the nozzle exit) and 31 mm on computation "31", or up to 45 mm on computation "45" (at transducers). Both resultant grids contain the same finely discretized zone in the jet where most of the noise sources are located. Grid 31 features a total of 8 331 765 cells and 58 377 688 faces, and grid 45 features 4 277 630 cells and 29 917 328 faces.

Modeling

Afterburning of propellant combustion products with air is modeled with a 17 reaction and 12 species kinetic scheme. It features the 6 major species in the combustion products, plus 5 intermediary species, plus N_2. Droplets of Al_2O_3 are modeled as an equivalent gas, in order to avoid a costly two phase computation.

Computations

Computation 31 is carried out on 1000 Intel Nehalem CPUs and requires a total of 16 h, and computation 45 requires 64 Intel Montecito CPUs during 120 h. The time step is set to 10^{-5} s and is slightly reduced at start-up. Pressure traces recorded on transducer 1 (20°) for 2D axisymmetric, 3D computations and experimental data are displayed in figure 21 and directivity is plotted in figure 22. IOP amplitude is much closer to the experimental data with 3D computations. Moreover, 3D computations lead to a better-estimated directivity on high angle transducers than previous 2D ones, highlighting the preponderant effect of the 3D nature of turbulence. Finally, decreasing the propagative grid size modifies directivity in the mid-angle direction only, while slightly changing the frequency distribution.

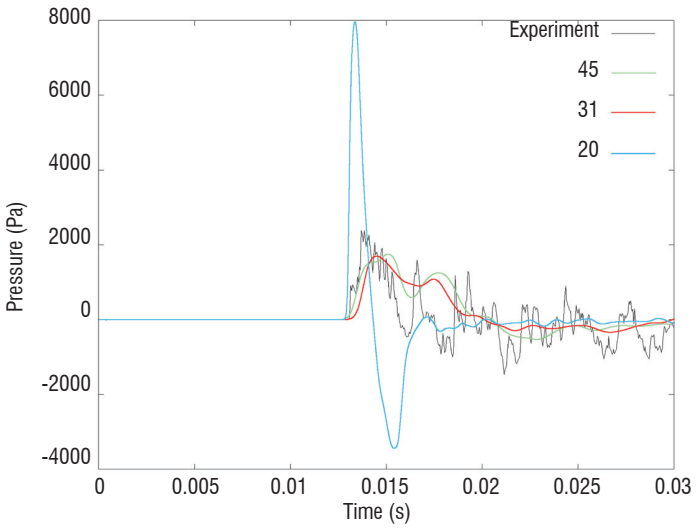

Figure 21 - Experiment/computation comparison (20°, 5 m)

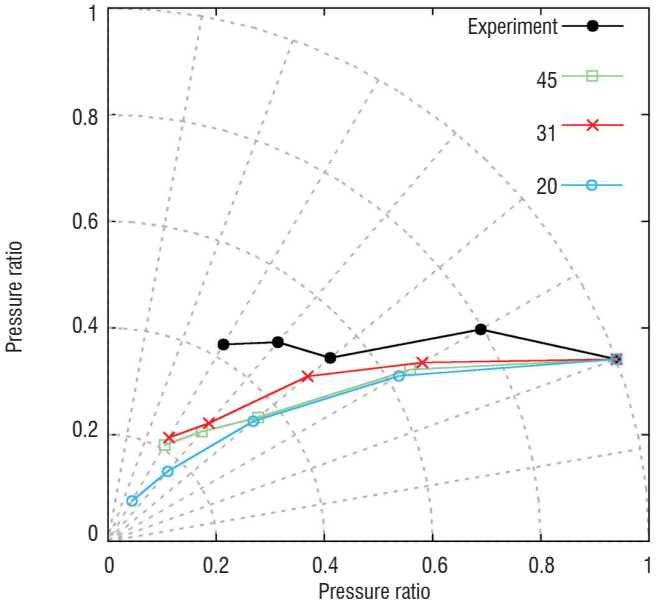

Figure 22 - Experiment/computation comparison - Directivity

Flame trench configuration (case II)

The second experiment focuses on the IOP and DOP: the jet is fired vertically in a water supplied flame trench.

Computational domain

The computational domain is built from a simplified geometry of the experimental set-up. It includes the combustion chamber aft end, the nozzle, the motor external structure and the flame trench (figure 23). The outside computational volume was limited to a quarter of a 3 m radius sphere, centered close to the nozzle exit.

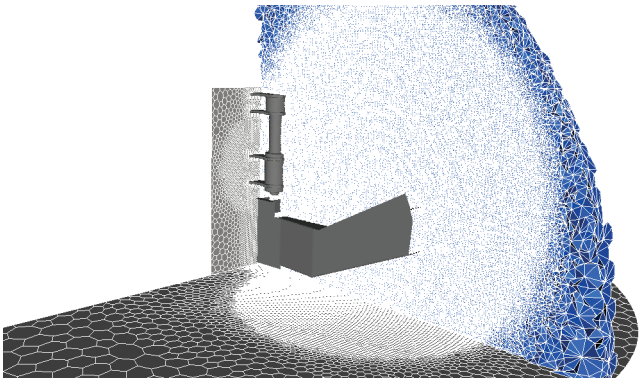

Figure 23 - Computational domain and grid

Grid

The volumic mesh is polyedric, mainly made of 14 sided elements. The grid includes a refined zone, centered on the flame trench exit, with a cell size of 23 mm (see figure 23). This size leads to an acoustic time step equal to 7.10^{-5} s (for sound speed of 340 m/s), consistent with an overall duration of 30 ms. The final grid comprises a total of 1 633 663 cells and 11 406 043 faces.

Modeling

The combustion products are modeled by a single species, called PROP; the ambient air, called AIR, is a perfect mix of O_2 and N_2; the species resulting from the combustion of PROP with AIR is called PROD, and is produced using an infinitely fast chemistry model (EBU/Magnussen type).

Water vaporization is taken into account by a model allowing the simulation of a two-phase flow (water plus vapor), as a mix of 2 distinct gaseous species: LIQ is an equivalent gas of the liquid state and VAP, its vapor. The inverse reaction (condensation) is not taken into account.

In addition, since the computations deal with a high density fluid, gravity is activated.

Computations

Three calculations are performed in order to compare the 2 main phenomena that are of concern (afterburning and gas/liquid interaction): 1 inert, without water (known as ID); 1 reactive, without water (known as RD) and 1 reactive, with water (known as RW). The inert computation is run deactivating the combustion reaction and the water-free ones are run deactivating the vaporization reaction. Water is taken into account as an initial condition (a water layer of 1.5 l is added at the flame trench bottom), without additional injection during the simulation. This is not fully representative since, in the actual experiment, water is injected during all the firing. All computations are carried out on 64 Intel Montecito cores. The calculation time steps are respectively set to 1.10^{-5} s, 1.10^{-6} s and 1.10^{-7} s. Figure 24 and figure 25 compare the calculated flows (13 ms after ignition) with and without water. The effect of water on the temperature field is particularly visible.

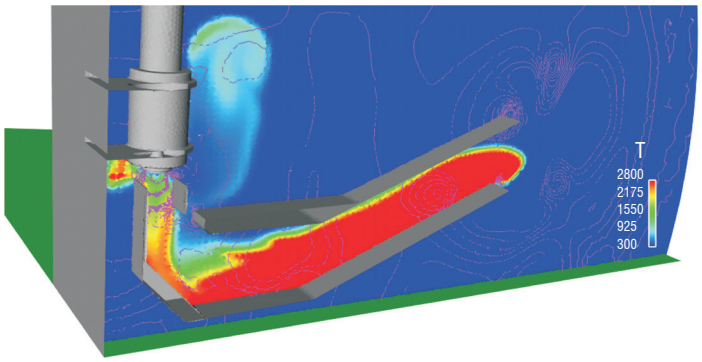

Figure 24 - Temperature field and isobar lines - Computation RD

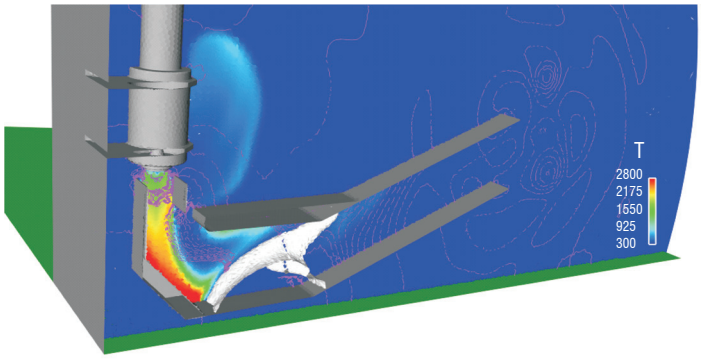

Figure 25 - Temperature field, isobar lines and iso water concentration - Computation RW

The transducer located at 5 m and 120° (figure 26) illustrates the separation of IOP (5 ms) and DOP (9 ms). The computation results are that IOP is reinforced by afterburning but that the water layer has no effect on this reinforcement. DOP is much less reinforced by afterburning and is, like IOP, nearly independent on water. Finally, a secondary DOP (14-21 ms) is observed in reactive computation without water. This secondary DOP is strongly mitigated in the reactive computation, with water in the flame trench, which reduces gas temperature near the exit.

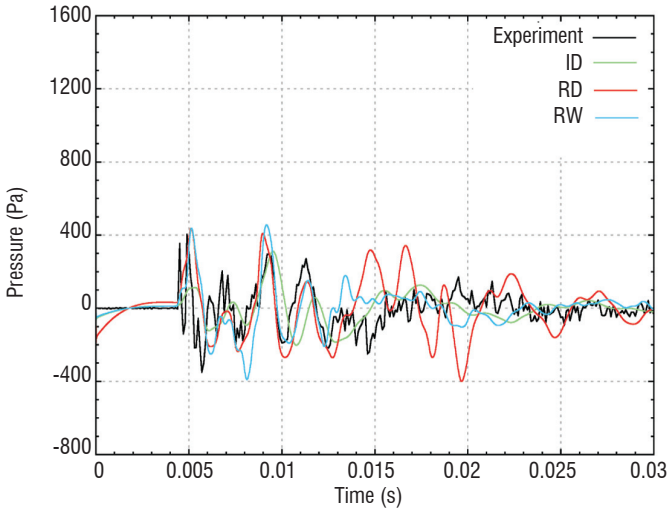

Figure 26 - Experiment/computation comparison (120°, 1.5 m)

Conclusion

This numerical study showed the benefits that 3D unsteady computations can bring to the understanding of IOP phenomena. However, case I has revealed that propagative area discretization seems to impact the solution at a lower order than the accurate simulation of noise sources located in the jet. Thus, efforts must concentrate on this point, in order to generate the complete range of frequencies observed during experiments. The case II results complement the analysis of physical interactions affecting the generation of different overpressure waves. The computations showed the important influence of afterburning and water injection on the blast wave. Further research is needed with more realistic models for combustion and water injection.

Jet noise prediction

Introduction

Numerical simulations are commonly used today in aeronautics for the analysis of noise generation and radiation problems. Jet noise, which is the main source of acoustic nuisance for an aircraft at take-off conditions, is especially investigated even though high computer requirements have restricted most of the existing work to simplified and isolated configurations. One of the challenges is thus to propose and assess the quality of a suitable simulation methodology, in order to target situations of industrial interest [52][59][6][4][25][60]. Onera has been working for several years to construct a hybrid Computational-Aero-Acoustics (CAA) approach to tackle this challenge. For instance, recent studies have made it possible to evaluate the proposed approach for the case of fluidic control of single stream isothermal and hot jets [25] and for the study of installation effects in the

case of a high by-pass ratio dual stream nozzle [60]. After presenting the details of the constructed approach, the results obtained for the two above mentioned cases will be presented briefly.

Computation methodology

The hybrid CAA approach, which is being investigated at Onera, consists in associating a Large Eddy Simulation (LES) of the jet flow to an acoustic integral formulation used to reconstruct the noise radiated to the far field. In sizing the requirements for such complex computations, the following points were considered:

• Firstly, the actual geometry must be reproduced in the computations. In particular, the exact geometry of the nozzles must be simulated in order to avoid both guessing the jet inlet conditions and forcing the jet flow to initiate the jet turbulence. Another important consideration is that most noise reduction devices involve the modification of the nozzle geometry itself (chevrons, serrations, micro-jets, etc.) which must be reproduced in the computations. In addition, it is desirable for the computations to be capable of taking into account the installation effects, which involve the nozzle surroundings (mast, pylon, wing, etc.). These geometrical requirements bear some consequences on the choice of the numerical schemes, which must be robust enough to accommodate complex, boundary fitted grids. In practice, upwind schemes of the MUSCL family were retained.

• Secondly, the computation duration, in clock time, should be short enough to allow parametric studies to select the most efficient nozzle arrangement. This implies some choices in terms of grid size and the related resolved frequency range of the LES simulations. In this regard, a deliberate choice was made to perform the LES computations with the smallest grid size compatible with the objective of capturing the main noise producing structures. A priori analysis showed that the smallest upper frequency should be of the order of St $= 0.5$ (St being the Strouhal number, based on nozzle characteristic diameter, D_j, and exit velocity, U_j). Moreover, an additional grid requirement came from the need to properly resolve the intense shear layer generated at the nozzle exit. These requirements, combined with the properties of numerical schemes, provided the necessary rules to design the grid in the jet noise producing regions. These rules can be applied to any configuration with the guaranty of similar flow resolution. This is an important result to ensure the meaningful comparison among different designs.

• Thirdly, the deliberate choice of tuning the computations toward actual geometries, even at reduced scale corresponding to available industrial wind tunnels (roughly 1/10), placed the computations in the high Reynolds number range (above 10^6) where the jet noise has a broadband, stochastic like, behavior. This implies that the time series produced by the computations and used to post-process the results must be long enough to avoid undesirable statistical bias. In practice, time series in excess of 100 D_j/U_j must be provided by the computations.

• Finally, in regard to the above requirements, an implicit time integration scheme appears to be highly desirable. Indeed, it rapidly appeared that the smallest grid size was required at the nozzle exit to resolve the sheared flow. These small cells would drive an explicit time step to excessively small values rendering the overall computation unaffordable. Considering that the initial high shear regions should be weakly affected by acoustic wave propagation, it was assumed that these cells could be operated at a local CFL number higher than unity, provided an implicit scheme could be used. Of course, thanks to grid stretching, the regions of high acoustic activity would be operated at a local CFL number below unity for consistent acoustic wave propagation computation.

From the analysis summarized by the points above, it appears that the CEDRE solver possesses many qualities to be retained as the work horse for jet noise studies. Indeed, it offers a wide range of robust and accurate second order MUSCL schemes, combined with several efficient implicit time integration schemes (from first to third order). Moreover, its polyhedral mesh capability makes it possible to combine many types of grid elements, to design properly tailored grids. In the course of these studies, started in 2005 [28], a common grid arrangement was defined: a structured hexahedral grid was designed to accommodate early sheared regions as well as the noise producing regions of the jet flow. Thanks to the CentaurSoft grid generator, this structured patch was embedded into an unstructured grid that made it possible to precisely describe the nozzle geometries with no limitations or penalties associated with particular arrangements.

Considering the acoustic part of the aeroacoustic simulations, the choice was made to rely on a surface integral acoustic solver. The Onera KIM code [42] was retained. Early studies showed the importance [3] of properly defining the surfaces onto which the LES solution was stored and of providing the necessary cross checking capabilities to avoid spurious results. In particular, the length and position of the surfaces were found to be of crucial importance and several surfaces were systematically used to ensure that the far field results were not dependent on particular surface arrangement. In the course of these validation studies, it was shown that the Ffowcs-Williams and Hawkings integral formulation (FW-H) was better suited to the case of hot jets and that surface length should be in excess of 20 D_j. The question of the closure of these surfaces was also studied and it was concluded that open surfaces could be safely used, provided that they were long enough.

This aeroacoustic methodology has been extensively tested at Onera against numerous configurations that were experimentally tested and provided a high level of confidence in the quality of the computed aerodynamic flow, as well as the near field and far field acoustic solution [33][34][40][61].

Computation results

To illustrate the above detailed methodology, two recent computations are presented hereafter. The first one concerns installation effects and the second one concerns noise control by micro-jets.

Case I: Installation effects (pylon) for a double stream nozzle

Following studies on several double stream nozzles, a first step was taken toward the study of installation effects by introducing the mast/pylon arrangement. The grid is presented in figure 27.

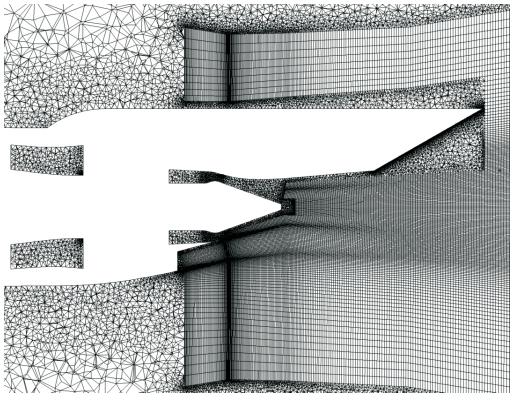

Figure 27 - Detail of the grid for the pylon configuration

The pylon region is cut into the structured hexahedra grid patch and the acoustic surfaces (figure 28) are placed in this patch, over the pylon. The grid is made of over 10 million cells and the computation is run on 64 cores of the Onera Itanium cluster. The total clock time was 360 h.

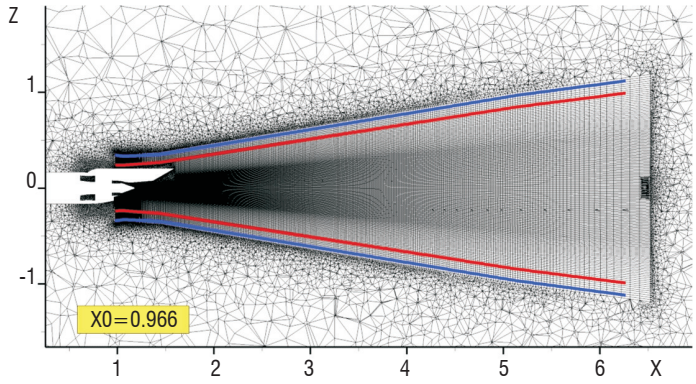

Figure 28 - Positions of the acoustic FW-H surfaces in the structured patch

The results showed good agreement with measurements performed during the course of the EU VITAL project [60]. In particular, the effects of the pylon on the jet flow (figure 29) and on the radiated noise (figure 30) were properly recovered by the simulation.

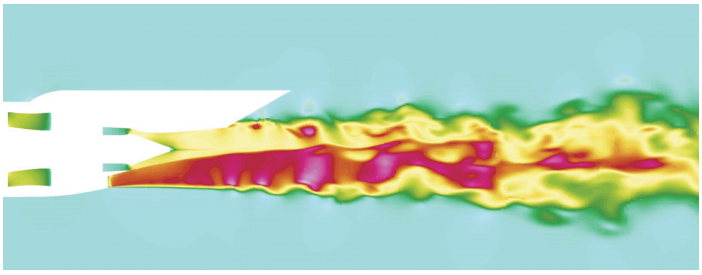

Figure 29 - Instantaneous Mach number field

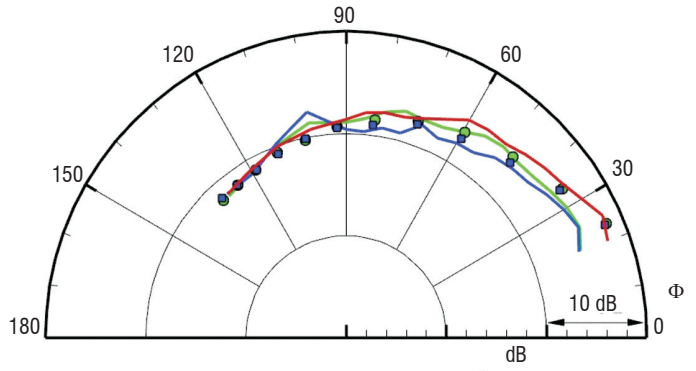

Figure 30 - Experimental (● sideline; ■ flyover) and computed (– sideline; – flyover; – without pylon) OASPL on the range [200 Hz ; 25 kHz]

Case II: Noise control by micro-jets

Recent original works were concerned by the effects of micro-jets as a means of reducing jet noise. A single stream nozzle (from the EU JEAN project) was used and 12 micro-jets were placed in the structured grid patch around the nozzle exit. Micro-jets were not resolved in the simulation, since it would have rendered the overall computation unaffordable. Instead, source terms were added in the simulation thanks to an ad hoc model to reproduce the injected mass, momentum and energy [25]. Each micro-jet was given a source characteristic placed in one cell of the computation (cell size was chosen to represent the actual size of each micro-jet of roughly 1 mm). Continuous or pulsed micro-jets were tested in the computations with significant results [25]. The grid arrangement is presented in figure 31.

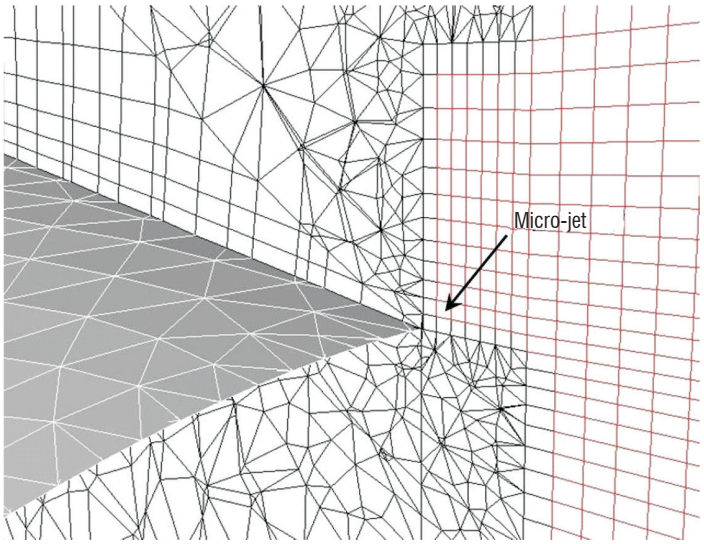

Figure 31 - Detail of the grid and micro-jet location at the nozzle lip

The effect of continuous micro-jets on the jet flow is illustrated in figure 32. The micro-jets are clearly found to modify the jet flow, in agreement with experimental observations. The effect on the radiated far field is also quite well reproduced by the simulation (figure 33).

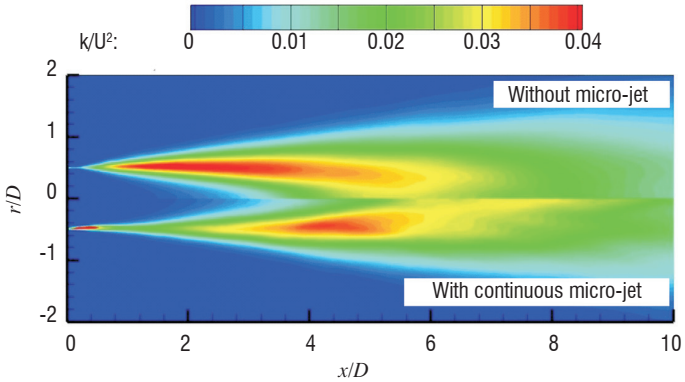

Figure 32 - Effect of continuous micro-jets on the mean turbulent kinetic energy for a hot jet case

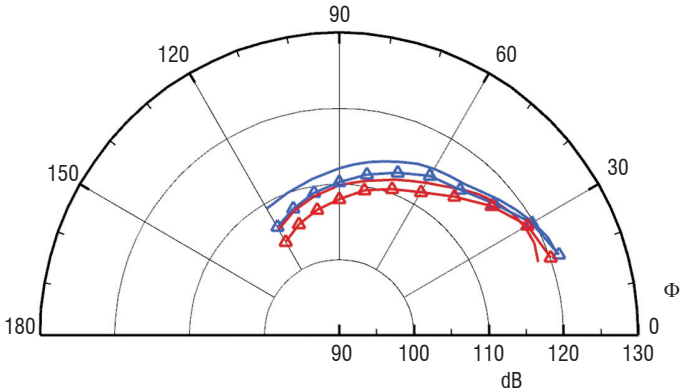

Figure 33 - Predicted directivities without and with continuous micro-jets, 30D from the nozzle exit. Isothermal jet: — baseline; –Δ continuous micro-jets. Hot jet: — baseline; –Δ continuous micro-jets

Conclusion

The methodology presented proved to yield valuable results in predicting and controlling jet noise from civil aircraft. Future work will address configurations of increasing complexity, as well as the evaluation of possible control strategies. Evolutions of the CEDRE code, such as moving grids and higher order schemes, etc., will notably benefit this application field.

Flow separation in an over expanded nozzle

Introduction

The ATAC nozzle is a planar nozzle designed to investigate the reacting flow, when operating in over expanded conditions, i.e., with a back pressure higher than the theoretical nozzle exit pressure [38]. This experiment aims to reproduce the flow separation occurring in rocket nozzle extensions on the ground and at the beginning of the flight. A detailed review on nozzle flow separation can be found in [24]. In such conditions, outside air engulfs the extension and can burn with the remaining reducing species (unburnt H_2 for instance) of the hot gases coming from the combustion chamber, creating additional thermal fluxes. The particular features of this test case are: a very high ratio between the exit and throat heights, an additional H_2 injection at half of the divergent length and the existence of both experimental OH visualizations and wall measurements. In this work, numerical simulations of this test case are carried out with the CEDRE code. The purpose of this study is to evaluate two approaches, steady RANS and unsteady DDES by comparison with the experiments. First, the modeling used and the numerical methods are briefly described. Then, the computational grid and the conditions of the computations are presented. Finally, both averaged and instantaneous results are compared to the experiments and discussed.

Physical models and numerical methods

Two approaches are used for turbulence modeling: a steady RANS approach with the k-ω SST model and an unsteady DDES approach (see [50] for a presentation of the approach implemented in the CEDRE code), which allows the attached boundary layers to be treated in RANS while switching to LES in the separated regions. The mixture is composed of seven species (H_2, O_2, H_2O, H, O, OH, N_2). The species destruction/production terms are obtained thanks to a 7 reaction kinetic scheme [16]. Apart from the general numerical methods used in the CEDRE code, Roe's flux difference splitting associated with a MUSCL interpolation is employed for the advective fluxes. This method results in a second order spatial accuracy (third order on isotropic mesh). The time integration is carried out using a first order Euler implicit scheme, with local time stepping to speed up the convergence of the RANS simulations and a global time step with a second order sub-iterated Gear scheme is employed for the DDES computation.

Computational grid and conditions of the computations

To perform the simulations, we chose to separate the computational domain into three zones, computed independently. This separation and some views of the structured grids are illustrated in figure 34. Such a separation is made possible by the supersonic nature of the flow in the upstream nozzle (zone 1) and injector (zone 2). Thus, the imposed conditions in the inlet sections of the over expanded region of the nozzle (zone 3) are given by the results of the steady RANS computations of zones 1 and 2. Approximately the size of the meshes of zones 1, 2 and 3, they are 1.5 million, 1 million and 6 million grid cells respectively. In zone 3, RANS and DDES computations are performed. Concerning the boundary conditions, the far field and the outlet correspond to pure air at ambient pressure and temperature. The composition of the hot gases in the upstream nozzle inlet is obtained thanks to an equilibrium computation at the given pressure, temperature and mixture ratio. In these computations, we aim at reproducing the conditions referred to as "P=25 bars, higher Rm, H_2 injection" in [38].

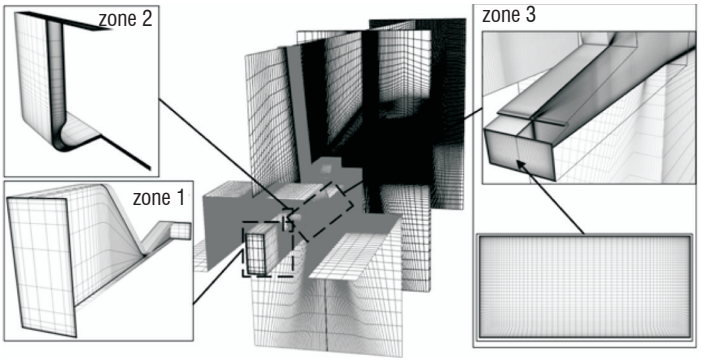

Figure 34 - Views of the meshes in the three different regions given by the separation of the computational domain

Results and discussion

First, the time averaged OH emission throughout the span wise direction is illustrated in figure 35 and compared to the equivalent OH mass fraction visualizations for RANS and DDES. In this figure, one can notice that DDES results match the experiments better, since the reacting region is wider than that for RANS, where a clear diffusion flame is produced downstream of the separation in the mixing layer. Indeed, in reality, the reacting region oscillates in such a way that the shape evidenced in RANS cannot occur. Moreover, if we compare instantaneous OH mass fraction screenshots (DDES) to PLIF-OH measurements in the mid-span section, one can notice that the particular behavior of the flame is well reproduced by the computation.

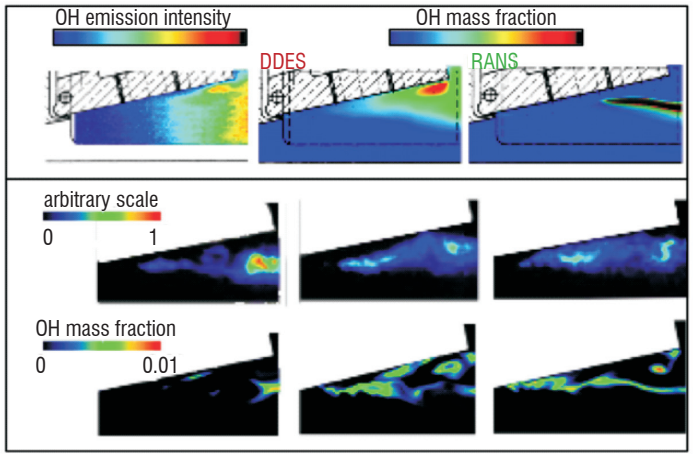

Figure 35 - (top) Averaged OH emission intensity in the spanwise direction, compared to the computations (bottom) Instantaneous PLIF-OH visualizations compared to a sequence of OH mass fraction in the mid-span section (DDES)

Concerning the wall measurements, one can compare the averaged and fluctuating pressure profiles in the second half of the extension (downstream of the injection) to the pressure measurements obtained during the campaign. These profiles are displayed in figure 36 and figure 37. It can be pointed out that the results of our simulations are in fair agreement with the measurements for the averaged pressure. Nevertheless the RMS pressure fluctuations are clearly overestimated compared to the measurements. Such a discrepancy can be explained by an insufficient spatial discretization in the separated region.

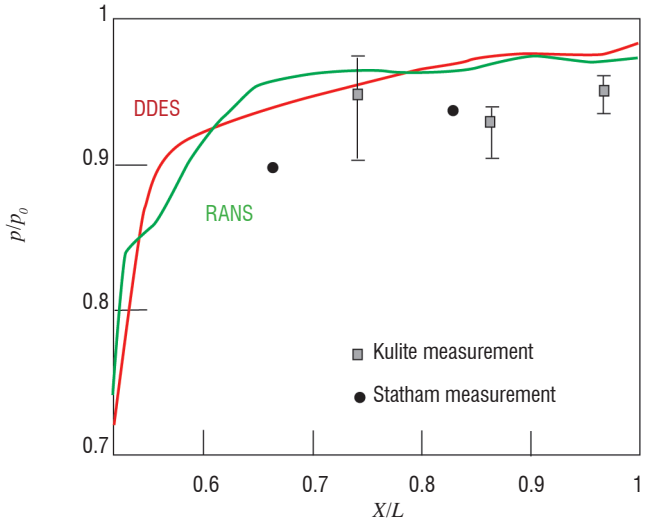

Figure 36 - Averaged wall pressure along the upper wall

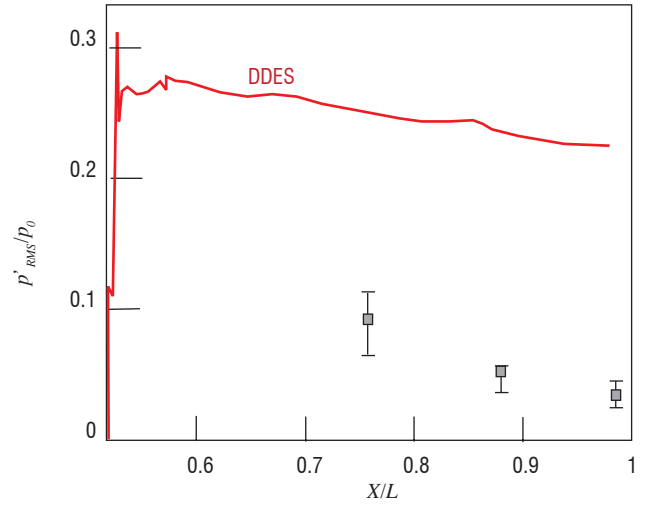

Figure 37 - RMS fluctuation of the wall pressure

Conclusion

Both steady RANS and unsteady DDES computations of the reactive flow inside an over expanded planar nozzle were successfully carried out and compared to the available experiments. This comparison highlights that RANS is unable to take into account the strong oscillation of the flow, which results in a poor estimation of the reacting region contrary to DDES, which is in fair agreement with the measurements for both averaged and instantaneous flow fields. Moreover, wall pressure profiles are in good agreement with the experiments for both methods. For DDES, the pressure fluctuations are overestimated. Further work is required to investigate the nature of the flow oscillation and the origins of this overestimation.

Aircraft and helicopter icing

Introduction

Icing occurs when an aircraft flies through clouds in which super cooled droplets are suspended in the atmosphere, with an ambient air temperature below the freezing point. The droplets impinge on the aircraft surfaces and freeze, leading to ice accretion. The resulting change in the aircraft geometry can modify aerodynamic characteristics (loss of lift, rise of drag), can affect the ability of the probes to provide accurate measurements, can block helicopter moving parts, can clog air intake or even damage the engine by ice ingestion, and in the worst scenario can cause a complete loss of the control of the aircraft or rotorcraft.

Airframe icing is therefore a topic of great interest for the aerospace industry and, more particularly, for airframers, because it deals with the safety and efficient operation of aircraft under all weather conditions. Keeping in mind the expected increase of airplane traffic in the coming decades, it seems unavoidable to reduce the rate of occurrence of ice-related incidents in order to maintain public confidence in air transport. For helicopters, customer needs are increasing for flight into icing conditions with smaller aircraft, for which capability substantiation is a key challenge.

In order to comply with certification regulation rules (CS25/CS29), airframers must show that the aircraft is able to fly safely in icing conditions. However, the entire icing envelope cannot be flight-tested and icing tunnel tests are time and cost consuming. Therefore, airframers, with the support of industrial partners, research institutes or universities, have developed numerical methods and tools to cover their needs.

Computation methodology

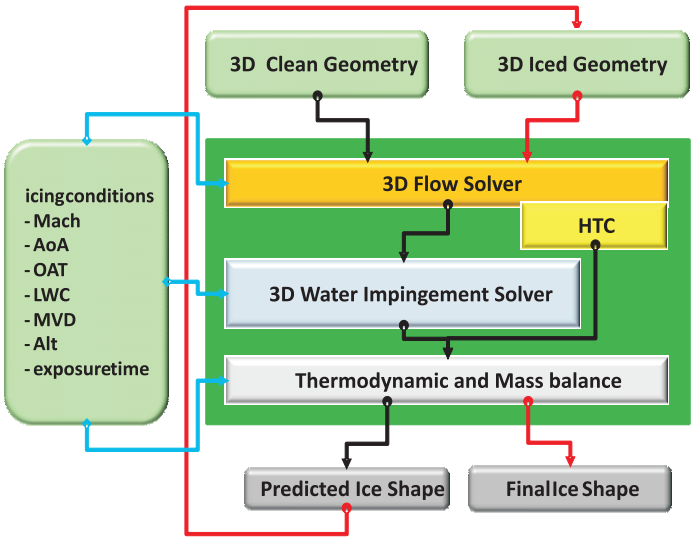

Figure 38 - Flow chart describing the predictor/corrector method to obtain a final ice shape

A recognized general methodology [32][9][31] used for the simulation of ice accretion is based on the successive computation of air flow, water droplet trajectories, collection efficiency, heat transfer balance and accreted ice. Figure 38 presents the general flow chart of the ice accretion process. The flow field and associated convective heat transfer are computed using an inviscid ap-

proach (Panel method, potential method, Euler method, etc.) coupled with boundary layer calculation or a viscid approach (RANS). The balance of forces acting on the droplets determines their trajectories and the collection efficiency coefficient β. Using these inputs, the resolution of the thermal and mass balance makes it possible to determine the ice thickness and then the ice shape on the considered surfaces.

All the modules that take part in the ice accretion process are usually included in a comprehensive ice accretion suite (LEWICE, ONICE2D/3D, etc.). The use of one module in a stand-alone mode or/and the replacement of one module by another is not obvious and not secured. Though such a way of working is acceptable for simple two-dimensional modules, the gradual replacement of two-dimensional methodologies by three-dimensional methodologies has led the partners of the project to ask Onera to build a modular ice accretion suite, enabling the partners to implement the modules in their own CFD environment [26][8][7] in a secured manner. Such a modular way of working offers the possibility of rationalizing the set of tools used inside an organization and then to reduce the maintenance and the associated cost.

The ONICE3D ice accretion suite satisfies these requirements. Interoperability is ensured through a CGNS [1] neutral layer. In order to ensure uniqueness and traceability, a restriction to the CGNS standard has been defined for icing purpose. Under this constraint, an in-house solver can be substituted to any of the specific components of the suite, as suggested in figure 39.

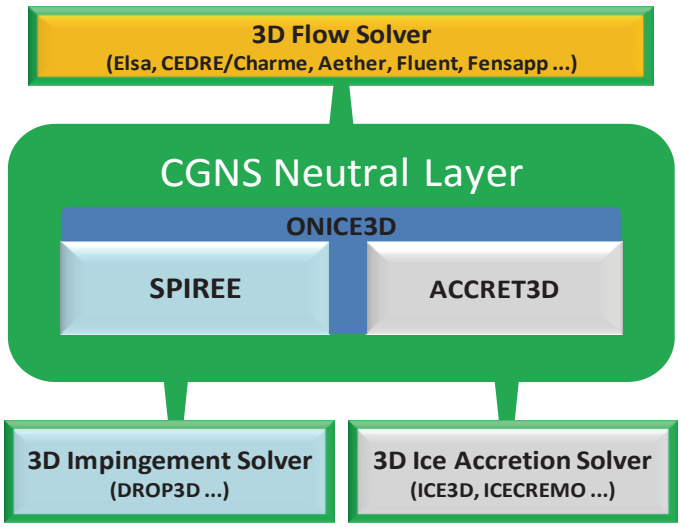

Figure 39 - ONICE3D components and the possible interoperability with other non-Onera components

Application to ice prediction on a 3D swept wing

The first test case is representative of a 30° swept airfoil (figure 40) and has been selected because some experimental results on water catch collection and ice accretion are available [39][41]. Among the various atmospheric and flight conditions tested during the icing campaign, one of the cold cases is presented. The atmospheric and flight conditions used for this reference case are the following:
$V_\infty = 67\ m.s^{-1}$, $T_\infty = 243\ K$, $P_\infty = 1013\ hPa$, $AoA = 0.0°$,
$LWC = 1.10\ g.m^{-3}$, $MVD = 20\ \mu m$

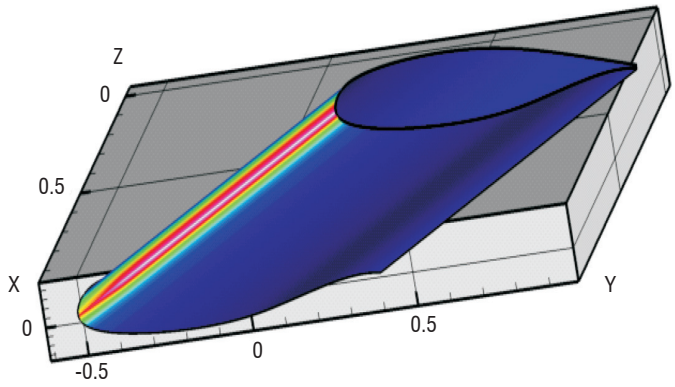

Figure 40 - Water catch collection coefficient distribution on the wing (SPIREE computation)

Figure 41 presents a comparison between SPIREE computations, Drop3D computations (Airbus code, green curves) and experiments for the classical water catch efficiency coefficient, as a function of the curvilinear abscissa. The effect of droplet diameter distribution, mono-disperse or Langmuir D, is also presented. The overall comparison shows that all computations reveal the same trend: the maximum value of the water catch collection coefficient is underestimated (value around 0.40 against 0.55 for the experimental reference). Lagrangian approach (not shown here) gives similar results. In a coherent way, the use of Langmuir D distribution improves the results near the impingement limits.

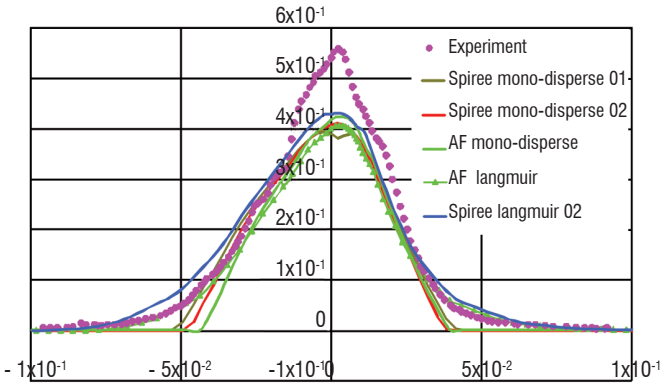

Figure 41 - Water catch collection coefficient: comparisons between reference and 3D Eulerian simulations

Figure 42 presents a close-up of the liquid water content normalized by its up-stream value. The absence of water is revealed by blue color map close to the profile. Values above unity show over-concentration that occurs when droplet trajectories are concentrated due to the profile deflection.

For the ice accretion comparison, the flight and atmospheric icing conditions slightly differ from the previous ones. The main difference is that the angle of attack is about 2.00° instead of 0.00°. Figure 43 shows the comparison between reference and numerical results. The predicted shape is in a rather good agreement though some discrepancies exist: ice thickness is 15% over estimated and the predicted limit of ice accretion is wider. However, the corrected shape should improve those results when applied.

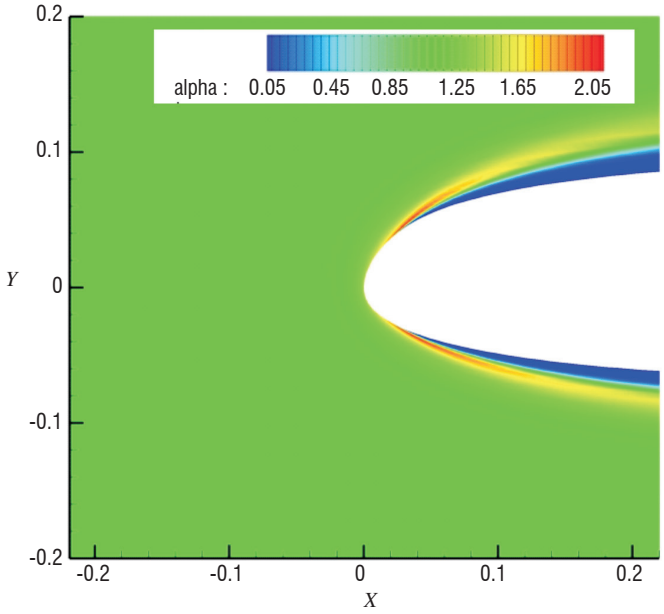

Figure 42 - Iso-contour of liquid water content distribution normalized by the up-stream value

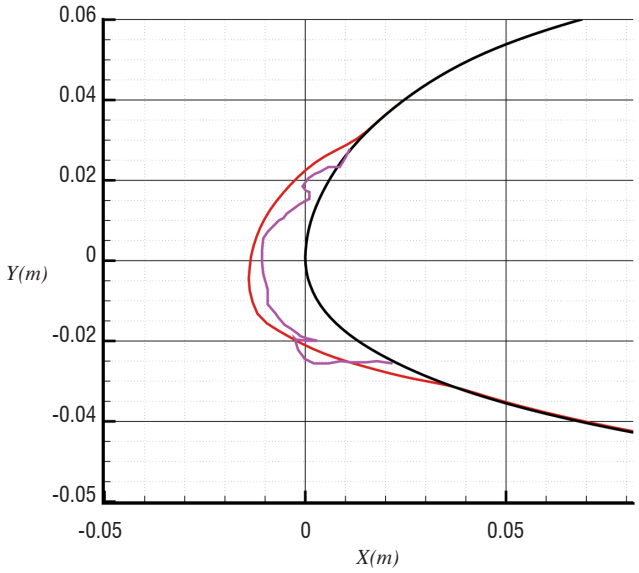

Figure 43 - iced profile normal to the leading edge

Application to ice prediction on a 3D air intake

The second test case is representative of a helicopter air intake. Under icing conditions, ice accretion can clog the air intake or damage the engine by ice ingestion and can cause a complete loss of control of the rotorcraft. In order to avoid this kind of damage, the air intake must be protected by an anti-icer. This anti-icer is designed to fully evaporate the super-cooled liquid water droplets that impinge. Usually, it is done by electrical resistor layers.

The atmospheric and flight conditions used for this reference case are the following:
$V_\infty = 75\ m.s^{-1}$, $T_\infty = 243\ K$, $P_\infty = 1013\ hPa$, $LWC = 0.80\ g.m^{-3}$, $MVD = 40\ \mu m$

Figure 44, figure 45 and figure 46 present the pressure distribution, the water catch collection coefficient distribution and the ice thickness distribution on the air intake surface respectively. These results

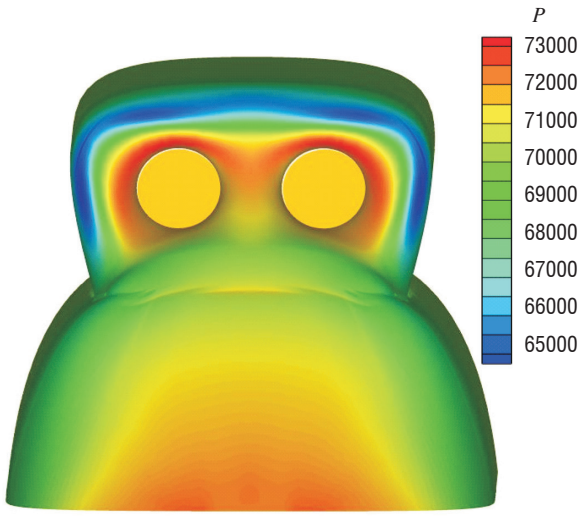

Figure 44 - pressure distribution on the air intake surface

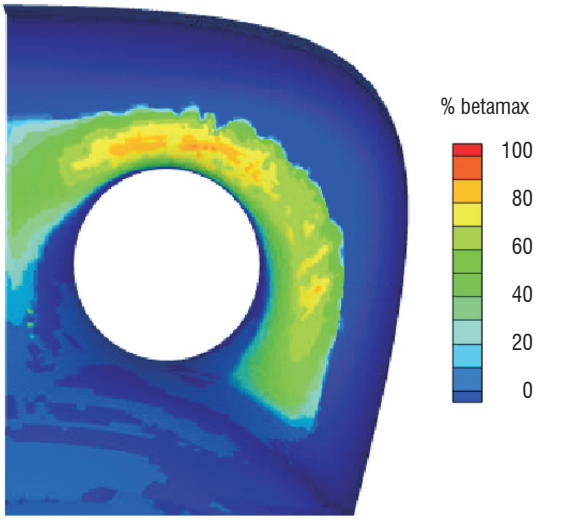

Figure 45 - water catch collection coefficient with a maximum value of 0.65

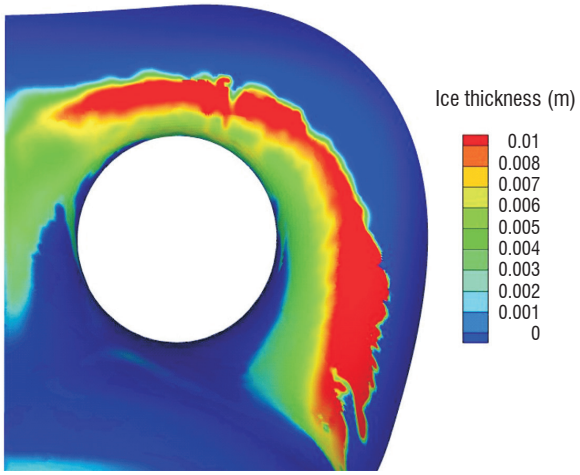

Figure 46 - ice thickness on the air intake surface

have been obtained using the CHARME solver for the aerothermics, the SPIREE solver for the eulerian transport of water droplets and the ACCRET3D solver for the ice accretion.

Conclusion

Icing computations with a numerical suite including the eulerian solver SPIREE for water droplet transport have validated the choice of

this numerical approach. In the future, an optimization work will make it possible to reduce the computation time. Concerning modeling, the future developments will concern wall/droplet interaction (splashing, rebound, etc.), the use of a sectional approach for the droplet distribution and the extension of SPIREE to rotating configurations.

Flow instabilities in a solid propellant motor

Introduction

Instabilities in solid rocket motors are a critical issue. They are likely to involve thrust oscillations and consequently dynamic loads on the payload. Pressure oscillations in large segmented solid rocket motors are mainly due to the coupling of the chamber acoustics with vortex sheddings caused by hydrodynamic instabilities. These vortex sheddings can be caused either by the Taylor flow intrinsic instability (parietal vortex shedding, PVS) or by a shear layer instability in the wake of protruding inhibitors for instance (obstacle vortex sheddings, OVS).

An idea to reduce the coupling between vortex sheddings and acoustics was to give the inhibitor a 3D shape, shown in Figure 47, in order to make large vortices less coherent. It was tested twice in ARTA 03 bench firings [54] and a preliminary reduced scale experiment (1/15th LP6) has also been carried out at Onera. In the LP6 experiment, the inhibitor was made of metal, so that no deformation occurs and the shape is known precisely. The subscale LP6 experiment showed that pressure oscillations are strongly modified by the introduction of a 3D shaped inhibitor. The levels are lower than with a classical ring-shaped inhibitor. However, an instability bump remains with quite disorganized frequency changes. At the time of greatest instability (8.6 s), the oscillation level is still low but involves mainly the excitation of the second longitudinal acoustic mode.

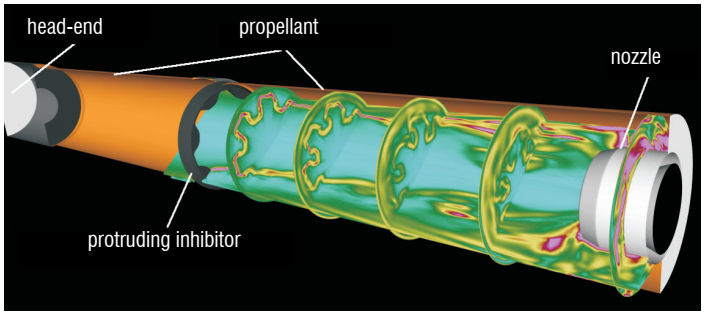

Figure 47 - Sketch of the motor and vorticity field

Numerical simulations of the experiment were performed at 8.6s, in order to provide a better understanding of the phenomena occurring in the motor (OVS and PVS interaction, enhancement of turbulence). A fixed geometry could be used, because aerodynamic and acoustic time scales are far smaller than burnback time scale.

Computation methodology

3D computations were performed with the Finite-Volume CFD code CEDRE. A single-phase approach was used (Navier-Stokes solver, CHARME), because the propellant used in the subscale experiment does not contain aluminum particles. One must keep in mind that in actual engines, aluminum combustion plays a major role in pressure oscillations (damping effect of the alumina particles, temperature increase, possible coupling between acoustics and aluminum combustion, etc.): for these configurations, a dedicated aluminum combustion model, available in CEDRE, must be used in association with a dispersed two-phase approach. Turbulence is treated with a MILES approach (the subgrid model is given by the numerical scheme diffusivity). The Euler fluxes are discretized with the Roe scheme. Second-order is achieved with a MUSCL scheme (with a Van Leer or a Superbee slope limiter). The temporal scheme is an explicit two-step Runge-Kutta scheme, second-order accurate.

The combustion of the propellant is simply modeled by an injection boundary condition at constant flow-rate q_p=12.025 kg/s/m^2 and temperature T_p=2688 K. Inert surfaces are treated as isothermal or adiabatic walls. In the first case, the surface temperature of the protruding inhibitor is T_{in}=500 K, the temperature of the head-end, aft-end and cylinder walls is T_{he}=2500 K.

The fluid properties are: molar mass M=24.394 10^{-3} kg/mol, specific heat capacity at constant pressure C_p=2153.8 J/K/kg, dynamic viscosity μ=8.07 10^{-5} kg/m/s and Prandtl number P_r=0.45.

The use of unstructured grids proved to be too dissipative to reproduce the low instability levels in this configuration with a reasonable grid size. With structured grids, computations using several grids of increasing size were actually necessary to obtain significant results: computations with too coarse grids exhibit no pressure oscillation. The retained mesh is an O-grid involving 4,288,000 hexahedral cells (12,917,280 faces). It is locally refined (down to 0.5 mm) in particular close to the propellant and close to the nozzle throat.

The integration was achieved with a Courant-Friedrichs-Levy number around CFL=0.3. For a satisfactory frequency accuracy, a large number of iterations is often necessary for pressure oscillation characterization. The computation was run on 64 ITANIUM cores. 2.5 million cycles were made in 180 10^{6}s CPU.

Numerical results

The computation exhibits pressure oscillations and vortex sheddings. The vorticity field downstream of the inhibitor is displayed in figure 47. A stronger interaction of both hydrodynamic instabilities, OVS and PVS, occurs where the inhibitor is shorter (at the top of figure 47). The vorticity field is perturbed by the 3D shape. Some OVS structures stemming from neighboring locations of the inhibitor interact strongly, as shown by transverse sections.

The RMS pressure oscillation level at the head-end is 318Pa if the Van Leer slope limiter is used. With a less diffusive approach (Superbee slope limiter), it increases to 425 Pa. This instability level remains low compared to the experimental measurement (2,900 Pa). However, as experimentally found, the signal is rather noisy and two dominant frequencies are identified near the first two longitudinal acoustic modes (1L and 2L, as shown in figure 48). However, the main peak in the experiment is locked on the 2L acoustic mode, whereas there is a little more energy around the 1L mode in the computation. The little discrepancies indicate that another refinement would be still necessary but the spectral behavior is globally satisfactory.

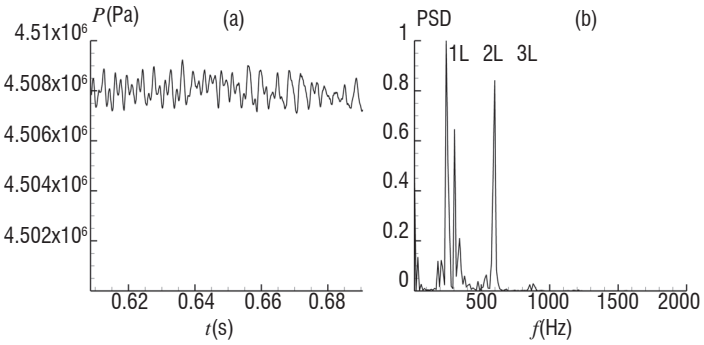

Figure 48 - Pressure at the head-end (a), power spectral density (b), computed with 2^{13} points, $\Delta f = 12$ Hz, $\Delta t = 10^{-5}$ s

Conclusion

The influence of a 3D protruding inhibitor in a reduced-scale solid rocket motor was studied by a numerical simulation with CEDRE Navier-Stokes solver CHARME. The instability level is lower than in the experiment: a more refined grid and/or a higher order spatial scheme should improve the instability level prediction. However, the spectral behavior is quite satisfactory. A strong second longitudinal acoustic mode (2L) is found, as well as some frequencies around the first longitudinal acoustic mode (1L). There are two types of vortex sheddings in the chamber : parietal (PVS) and obstacle (OVS) vortex sheddings. They interact weakly and the OVS vortices stemming from different heights of the inhibitor are in interaction, which is likely to enhance the turbulence intensity.

Combustion in a multipoint injection burner

Introduction

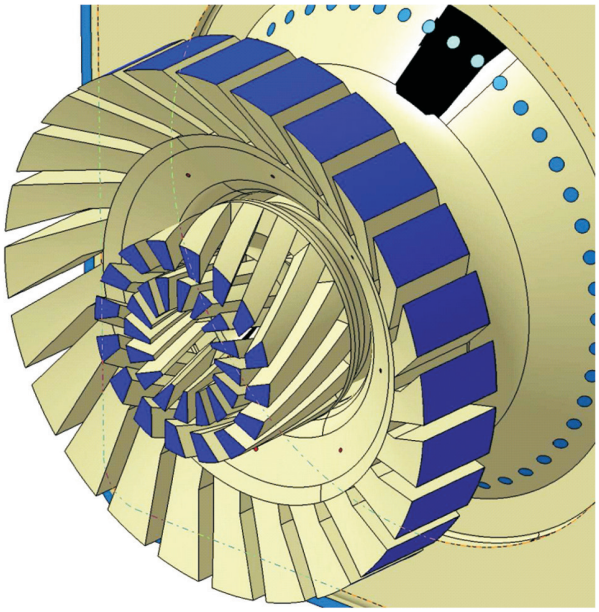

Figure 49 - Injector geometry

To comply with more and more stringent standards for pollutant emissions (NOx, CO, soot, etc.), new combustion chamber designs are required. A way to reduce pollutant emissions in the combustor consists in bringing close to each other a pilot zone and a low fuel air ratio combustion zone. This concept has taken shape through the Twin Annular Premixing Swirling (TAPS) or multipoint combustor [13] [53], in which fuel injection occurs from multiple points around or within an air flow undergoing a strong swirl. This concept initially developed by GE is now widely studied, in particular in Europe through EEC research programs as NEWAC (New Aero Engine Core Concept), Intellect D.M. (Integrated Lean Low-Emission Combustor Design Methodology) or TLC (Towards Lean Combustion). To improve and predict performance of such concepts, different experimental and numerical studies are carried out at Onera. An example of numerical study is presented in this paper.

The objective of the study is to simulate with the CEDRE platform, the 3D reacting diphasic flow in a combustion chamber fitted out by a multipoint injector (Snecma TLC injector, figure 49). The simulated operating condition corresponds to the approach stage, where the fuel (n-decane) flow distribution is 50-50 % between the pilot and the low fuel-air ratio combustion zone.

Computation methodology

The simulation is carried out in three steps. First of all, the 3D reacting diphasic flow is obtained with the coupled CHARME/SPARTE solvers (available in CEDRE platform) calculation. CHARME solves eulerian balance equations with a RANS k-l model. For the combustion modeling, we have used a one step infinitely fast Magnussen model [29]. The SPARTE (lagrangian) solver has been used for the tracking of the fuel droplets. The interaction between the liquid and the gas phases is taken into account through source terms in the eulerian balance equations of the gas. These source terms account for all the phenomena related to the fuel vaporization. For this kind of computation, ODFI flux difference splitting, associated with a MUSCL approach, is employed for the advective fluxes. This method results in a second order spatial accuracy. The time integration is carried out using a first order implicit Euler scheme, along with local adaptative time step.

In a second step, the flowfields so obtained (pressure, temperature, velocity and mass fraction of majoritary species) are post-processed with the PEUL+ solver to calculate soot volumic fraction and minority species such as NO, with a partially detailed kinetic scheme (127 reactions). Concerning the interaction between turbulence and chemistry, simulations are based on a method [64] that associates the eulerian resolution of the balance equations with the lagrangian resolution of a species PDF transport equation.

Finally, in post-processing of PEUL+ results, radiative transfer in the combustion chamber is solved with the ASTRE solver which is based on a Monte Carlo approach. We have taken into account radiation from CO_2, H_2O and CO gas species and soot in the infrared spectral range. The radiative properties of gas species are calculated with a band model (53 bands) formulated with a mean absorption coefficient (high pressure box model) and soot radiative properties are calculated on the same spectral discretization as a gas model with an expression of absorption coefficient that is assumed to be proportional to the volumic fraction and wavenumber. We have assumed furthermore that the media is without scattering.

All calculations have been carried out on a initial mesh constituted of 600000 tetrahedrons and 1200000 faces. For each step of the computation (CHARME/SPARTE, PEUL+, or ASTRE), parallelization has or has not been carried out. The following table summarizes the main characteristics of the three computation steps.

Solver	CHARME/ SPARTE	PEUL+	ASTRE
Number of processors	64	16	4
Kind of parallelization	Geometric domain	No	Optical path
Processor type	Montecito 1.6 GHz	SX-8R 2.2 GHz	Montecito 1.6 GHz
CPU time (h/proc.)	40	40	4
Convergence characteristics	-	50000 particles	10 million rays/proc

Main characteristics of the three computation steps

Computation results

Figure 50 and figure 51 present the temperature and pressure obtained with CHARME/SPARTE solvers in the combustion chamber. In the pressure field, streamstraces are also represented and show clearly the two recirculation bubbles led by the swirl injection system.

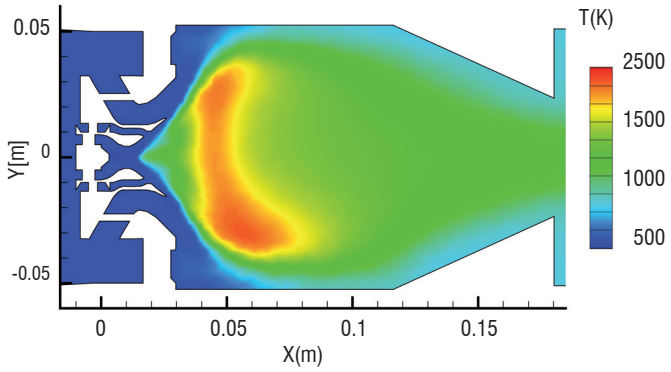

Figure 50 - Temperature field (longitudinal slice)

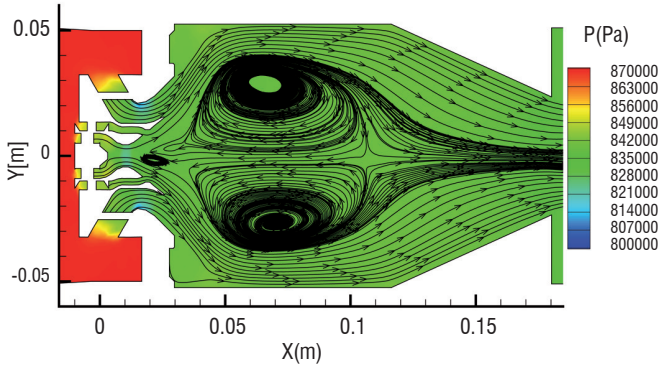

Figure 51 - Pressure field (longitudinal slice)

Figure 52 shows the NO mass fraction distribution obtained with the PEUL+ solver. The mass fraction is particularly important in the recirculation zone where temperature and residence time are high. The NO index in the outlet chamber is 4.42 g/(kg fuel), which is close to experimental data, 3.46 g/(kg fuel), measured on the M1 test bench (Onera/Palaiseau) under the same operating conditions.

Figure 53 presents the net radiative flux received by the walls of the combustion chamber. In our case, we have considered the walls as a black body emitting at 1000 K. The flux is particularly high on the system injection wall and on the side wall center.

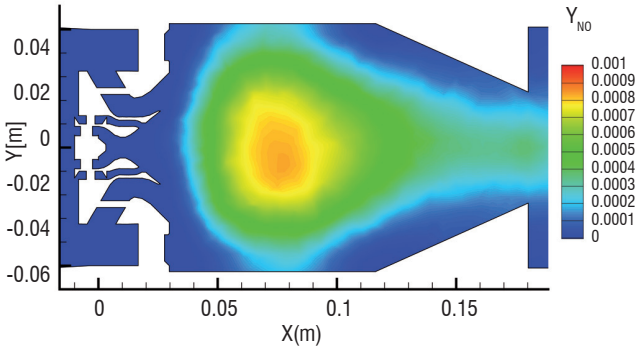

Figure 52 - NO mass fraction field (longitudinal slice)

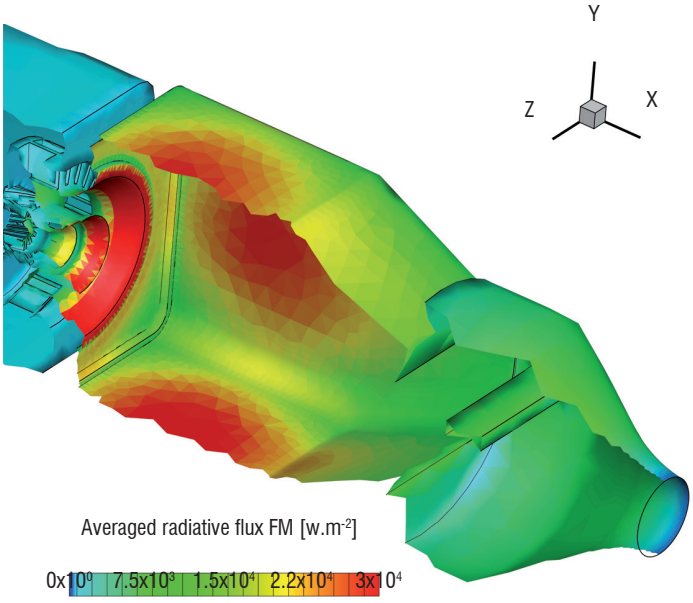

Figure 53 - Radiative flux distribution on the walls of the half combustion chamber

Conclusion

This study shows the ability of the CEDRE code to simulate a complex multiphysics flow in an industrial burner with realistic results. Nevertheless, this computation is only a first step since several points remain to be improved. First, even if the emission computation by PEUL+ uses a detailed chemistry, the flow calculation itself is based on a RANS approach with a basic one-step turbulent combustion model. Second, only a one way coupling is used between CHARME/ SPARTE, ASTRE and PEUL+ : in particular, temperature is overestimated, since radiative heat losses have not been taken into account in CHARME.

In future work, LES (Large Eddy Simulation) will be used in conjunction with a more realistic combustion model (such as Thickened Flame for LES). Furthermore, a two way coupling methodology between flow and radiation should be used soon.

Reacting flow in a research ramjet combustor

Introduction

The Research Ramjet Program has been initiated some years ago at Onera with two main goals: to provide a better understanding of the non-reacting and reacting flows inside a ramjet combustor and to validate models and CFD codes in order to have numerical tools able to predict ramjet combustor performances. For the first years, a specific ramjet combustor has been designed in order to build an experimental database for non-reacting and reacting flows. The configuration is a two-inlet side-dump ramjet combustor: the main combustion chamber of rectangular cross section is fed by two lateral rectangular cross section air inlets. In fact, according to this configuration, two three-dimensional research ramjet combustors were manufactured: the first one is dedicated to hot reacting flow experiments under realistic conditions (combustion mock-up, figure 54), and the second one, at scale 1.6 with respect to the combustion mock-up, is dedicated to cold flow experiments at atmospheric pressure (transparent mock-up, figure 55).

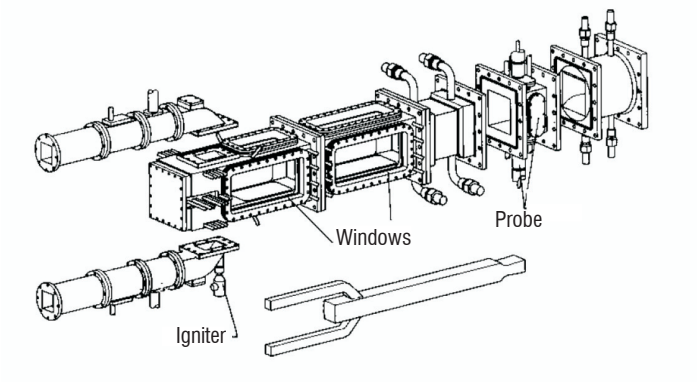

Figure 54 - View of the combustion mock-up

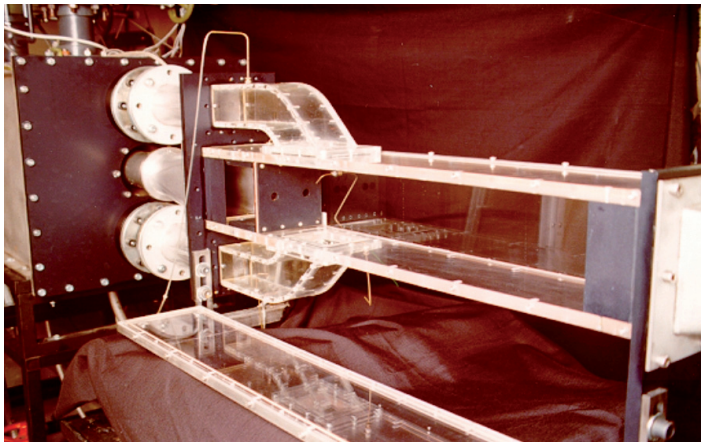

Figure 55 - View of the transparent mock-up

The combustion mock-up can be operated as a Solid Ducted Rocket (SDR) or as a Liquid Fueled Ramjet (LFRJ). In the first case, gaseous propane (representing the reducing gases coming from the gas generator) is injected into the head-end region of the combustor through two circular pipes. In the second case, liquid kerosene is injected from injectors located in the air intakes. We will focus here on the SDR operation only. Several flight conditions, with various equivalence ratios have been investigated. Experimental results using, for example, Particle Imaging Velocimetry (PIV), OH-PLIF (Planar Laser Induced Fluorescence) imaging techniques or gas sampling analysis are available [47].

The transparent mock-up is dedicated to cold flow visualizations. In the case of a SDR simulation, two pseudo-fuel holes (propane is replaced by carbon dioxide) are located at the head-end of the combustor. Low speed pseudo-fuel-to-air mixing process has been characterized by visualizations, PIV and gas sampling analysis [48].

The complexity of the flow structure observed in such a combustor has been analyzed in many studies [44][45][47][48]. Usually, one distinguishes: i) the head-end region (also known as “dome”) of the chamber, ii) the four corner vortices which connect the dome region to the rest of the chamber and, finally, iii) the rest of the combustor. The dome region is a recirculation zone which makes easier the mixing between air and fuel before the combustion, and the four corner vortices are essential for flame stabilization. Thus, having a numerical tool able to predict the flow features in those two regions is of primary importance.

Thanks to the huge amount of experimental data obtained, essential data is available to improve and validate numerical simulations of ramjet combustors. The main – and challenging – objective is to implement a predictive numerical tool, capable of:

- characterizing the global performances of ramjet combustors (combustion efficiency and pressure recovery);
- predicting the extinction of the combustor (and especially the lean blow-out);
- predicting the combustion instabilities.

Computation methodology

Reynolds Averaged Navier-Stokes (RANS) computations have been the first approach used to study the ramjet combustor. With this technique, only the mean flow field is resolved. Then, progress in Computational Fluid Dynamics (CFD) and increasing computer power have made possible the use of Large Eddy Simulation (LES) to study the ramjet combustor. This technique solves the filtered Navier-Stokes equations to describe the larger scales of turbulent flows, while only smaller scale effects are modeled. Although predictiveness of computations using LES approach is greater than the ones using RANS, the RANS approach is still extensively used for ramjet combustors because it is less demanding in terms of time and memory resources. Therefore, analyzing the advantages and limitations of RANS approaches and trying to improve them thanks to experiments, or LES computations, are two of the main objectives of the Research Ramjet Program. All computations have been performed with the compressible flow solver CHARME included in CEDRE.

For RANS computations, turbulence was modeled by a two-equation model, either k-ℓ or k-ω SST. No subgrid turbulence model was used in LES computations (MILES approach). For RANS and LES computations, combustion was modeled by an Arrhenius-type two-step chemical mechanism. For LES computations, two models including partial molecular mixing effects (TPaSR and EVM) were tested, without significant improvement of the results. For the RANS and LES approaches, combustion is initiated by performing a RANS calculation with an infinitely fast chemistry model. More detailed information on the modeling can be found in [44] and [45]. The computational domain – only a quarter of the mock-up due to the symmetry planes – is 3-D

and various unstructured grids, made of tetrahedra or hexahedra, and including or not the pre-injection box of carbon dioxide were used. The number of cells ranges from 200 000 to 4 000 000. A first-order Euler implicit time integration scheme, with an adaptative local time stepping for robustness, was used. Concerning the LES of the non-reacting case, the computational domain embraced the entire geometry and the grid was made up of roughly 3 000 000 hexahedra. An implicit second-order accurate Runge-Kutta method with Generalized Minimal RESidual (GMRES) resolution was used [45]. This approach is quite innovative for a LES computation and reduces the computation time significantly, compared to an explicit scheme. All those computations were performed on a 4-processor NEC SX–8R node. The CPU time ranges from 20 to 60 hours for RANS computations and reaches 960 hours for the LES computation.

Computation results

This paper presents the results concerning two cases, both relative to the SDR operation: the low-speed non-reacting air/CO_2 mixing in the transparent mock-up and the reacting air/propane mixing in the combustion mock-up.

Cold flow computations were compared to velocity and CO_2 mass fraction fields obtained during experiments. One of the most significant results is that all the RANS simulations implemented tend to over-predict, by a factor up to two, the CO_2 concentration in the head-end region, while the LES approach brings a real improvement (figure 56). In fact, for this non-reacting configuration, the flow is dominated by the oscillation of the impinging jets. In contrast to the RANS approach, the use of LES allows to simulate the unsteady behavior due to the air jets, which provides a more realistic and accurate description of the mixing processes in the dome region.

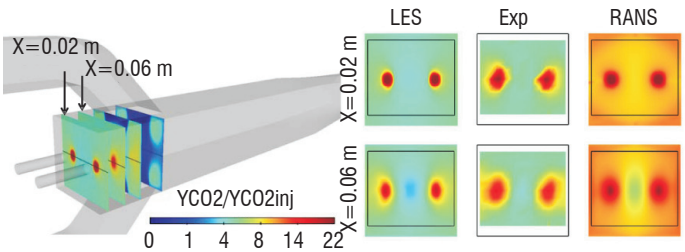

Figure 56 - Adimensionalized average CO_2 mass fraction fields in the dome region: comparisons between RANS (right), LES (left) and experiments (center) [44]

RANS and LES computations of air/propane combustion in the combustion mock-up have also been performed recently. The computed case corresponds to high altitude flight conditions, with an equivalence ratio $\Phi = 0.75$. The analysis of the LES results has allowed a better understanding of the combustion processes and has yielded information about the unsteady activity in the combustor (figure 57 and figure 58). As expected, the results of LES computations are in good agreement with experiment.

More surprisingly, some results of RANS computations are satisfying too: for example, the combustion efficiency and the mean velocity contours downstream of the air inlets (figure 59) were well predicted.

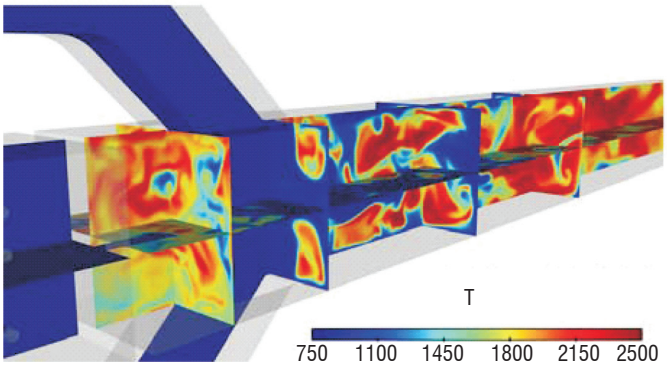

Figure 57 - Example of LES results: instantaneous temperature field

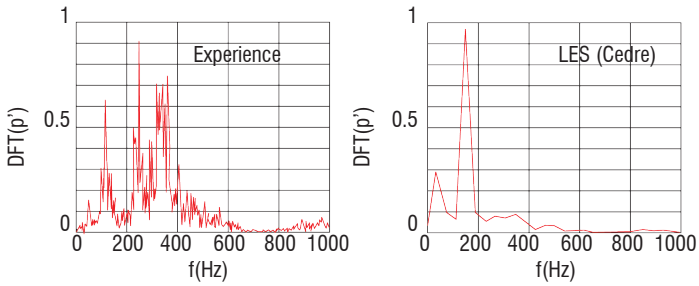

Figure 58 - Example of LES results: Fourier transformation of a pressure signal

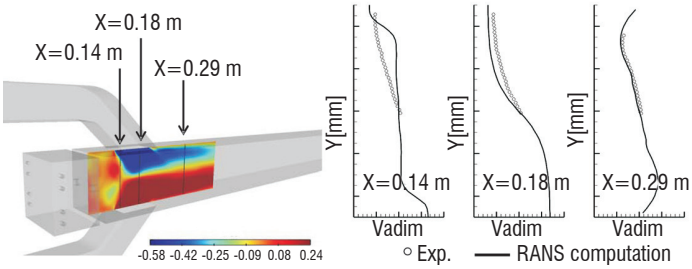

Figure 59 - Example of RANS computation result: adimensionalized transverse velocity contours – RANS vs. exp.

Conclusion

The comparisons between RANS and LES approaches for the computation of the flow in a ramjet burner has confirmed the decisive advantage of LES when the flow is governed by large scale unsteady phenomena, as the mixing process in the dome. LES is also expected to be the most appropriate approach to predict blow-out or combustion instabilities. However, some global performances of the burner can be predicted at a much lower cost, with a reasonable accuracy, using a RANS approach for stable conditions. The two approaches should therefore be used in a complementary way.

Combustion in the MASCOTTE cryogenic burner

Introduction

In the context of cost reduction and strong competition between space launchers, rocket engine design resorts more and more to simulation tools, in order to reduce design delays and development costs. These simulation tools require a detailed validation, which relies upon experimental means, such as the MASCOTTE test bench and advanced diagnostics [23]. The work described in this paper has been achieved in this context and within the fra-

mework of the CNES/Onera common program on liquid propellant rocket engines.

The purpose of this work is the simulation of the LOx/H_2 cryogenic combustion in subcritical and supercritical regime for the MASCOTTE test configuration. The MASCOTTE test facility has been developed by Onera for fifteen years to study elementary processes, such as atomization, droplet vaporization and turbulent combustion, which are involved in the combustion of cryogenic propellants. Several versions of MASCOTTE are available. In the experiments considered, the MASCOTTE test-bench is equipped with a subscale mono-injector combustion chamber of 50 mm x 50 mm square internal section. The chamber is equipped with two side windows, which are cooled by a helium film, for visualization and optical diagnosis purposes. Temperatures in the hot gas flow are measured using CARS techniques. The MASCOTTE injector is a coaxial injector, where liquid oxygen is injected at the center and gaseous hydrogen at the periphery. In this paper, we focus on the A-10 point for subcritical regime, which corresponds to an Oxygen/Fuel ratio of 2.11 and a chamber pressure of approximately 10 bar, and on the A-60 point for the supercritical regime, where the Oxygen/Fuel ratio is around 1.54 for a chamber pressure close to 60 bar.

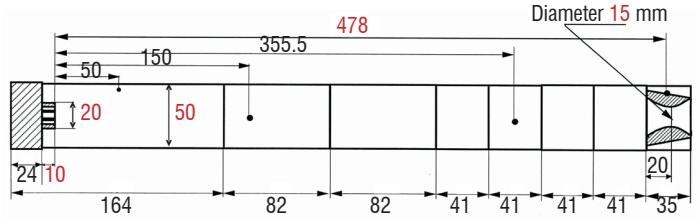

Figure 60 - Sketch of the MASCOTTE test-bench

Subcritical regime

Computation methodology

The simulation of the MASCOTTE test case is difficult because various complex physical processes take place in this reactive, turbulent, two-phase flow, such as atomization, vaporization, mixing and combustion. Thus, to compute this test case, a progressive approach was adopted. First, we simulated an equivalent version of MASCOTTE in 2D-axisymetrical gaseous configuration. Then, we investigated the influence of the various models of the CEDRE code on the flame shape in a 2D-axisymetrical two-phase flow configuration. From this study [37], we developed and validated a turbulent combustion model, based on mixing pseudo-reactions and kinetic reactions known as TPaSR for Transported Partially Stirred Reactor [35]. Turbulence was modeled by a two-equation k-l model, with a parameter set specially optimized for cryogenic combustion in a subcritical regime. The liquid phase was treated by the lagrangian solver SPARTE included in the CEDRE platform. Liquid oxygen injection is represented by a solid cone, along which droplets are injected. We showed that a non-uniform droplet distribution allowed a good coherence between the numerical results and the MASCOTTE data base. Nevertheless, some discrepancies still remain and they could come from the 2D simplification. Thus, the next step is the 3D simulation, using the optimized parameter set of the 2D simulation to complete the study.

For the 3D simulation, we meshed only 1/4th of the chamber with an unstructured grid composed of 665 600 nodes, 7.7 millions of faces and 3.8 million cells. For the first computation of this kind, the grid was not very refined, to assess the capability of CEDRE to treat such complex configurations. We used a second order interpolation at the face center, with a Van Leer limitation. The gradient computation is provided by a Green method. The numerical Euler fluxes are based on the ODFI flux difference splitting. The time resolution is one step implicit, with local time step. The simulation is performed on the scalar parallel Bull calculator. This cluster is composed of Intel Itanium 2 processors. We used 32 processors.

Computation results

Figure 61 represents the computed temperature field in the steady state. A slight asymmetry can be observed between the XY plane (observation plane) and the XZ plane (transverse plane): the flame opens with a wider angle and more quickly in the observation plane than in the transverse one. This is due to the cooling helium films, present only on the walls parallel to the observation plane (figure 62).

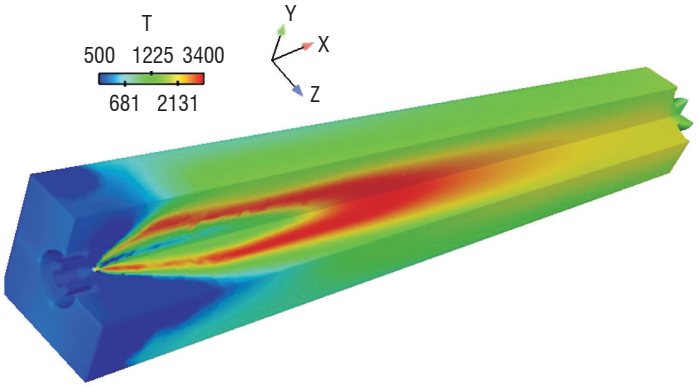

Figure 61 - Temperature field

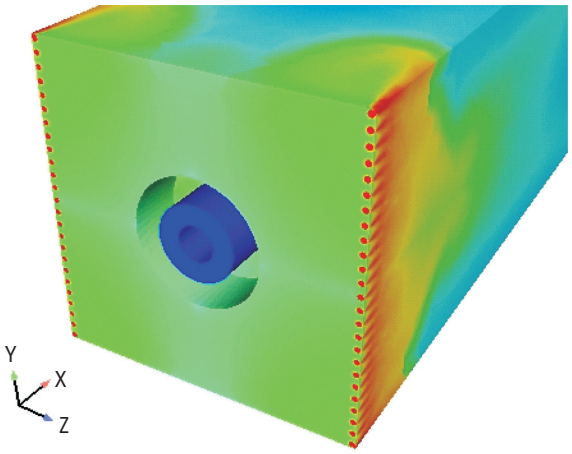

Figure 62 - Helium mass fraction

The effect of the helium films on the wall temperature is more easily visible in figure 6, where the temperature scale has been limited to 1500 K, which is the maximum value advocated by the window furnisher. One can see that the helium films are quite efficient, since the window temperature remains below this maximum value.

Figure 64 provides a comparison between simulation and experiment for the transverse evolution of temperature in the median plane, at the end of the chamber. There is a good agreement between simulation and CARS measurements. Nevertheless, some discrepancies remain in regard to the flame aperture shape, but to provide a significant comparison between simulation and experiment the computation should

supply radical OH emission like experimental images: this could be done by using ASTRE, the CEDRE radiation solver.

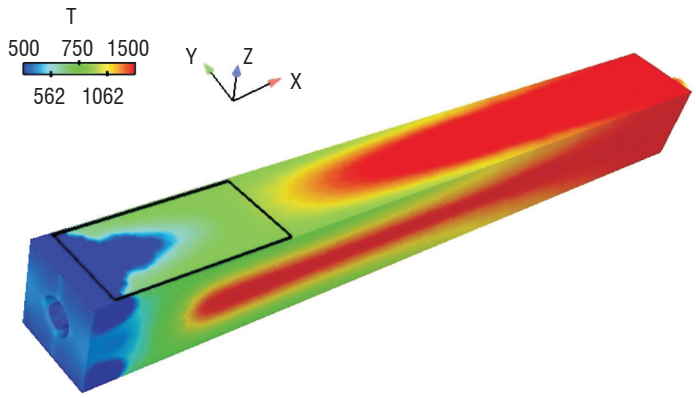

Figure 63 - Temperature field and window

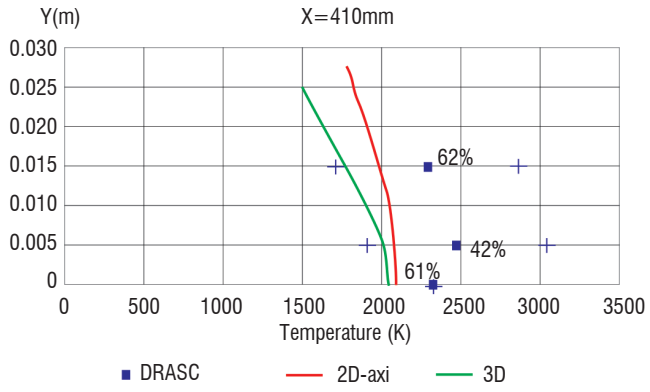

Figure 64 - Comparison CARS / simulation 2D-axi and 3D (Z=0, X = 410 mm)

Supercritical regime

Computation methodology

The simulation of the supercritical regime required the extension of the CEDRE code to real gas thermodynamics, in order to model the entire fluid phase (dense cryogenic injection as combustion gases) as a single monophasic medium. Following several authors [30][46], a Soave-Redlich-Kwong state equation was used for the computation of thermodynamical properties. In order to reduce the computational cost, the simulation was computed on the equivalent 2D-axisymetrical geometry of the MASCOTTE test bench. In this case, the liquid oxygen injection tube is included in the computational domain, rather than being represented by the solid cone frontier. Aside from the thermodynamic modeling, the assumptions made concerning chemical reactions and turbulence are rather classical: for the turbulence model, we used a k-l model without any parameter optimization and the chemical model consisted in a kinetic model using an Eklund scheme [16].

The 2D-axisymetric equivalent geometry was meshed with a light unstructured grid, composed of around 15 000 polygonal cells. This rather rough mesh is only refined near the injector, where the more representative real gas effect are expected. The choice of polygonal cells has been made to improve gradient evaluation through a least square method. Spatial interpolation, limitation, numerical fluxes and time resolution are the same as that used in the 3D subcritical computation. The simulation was performed on 8 quad core Intel Nehalem-EP processors of the scalar parallel SGI calculator.

Computation results

Figure 65 and figure 66 present details of the density and temperature fields in the wake of the injector. Cold oxygen injection reaches liquid like densities and the flame stabilizes around the dense core. The high density gradients that may arise from turbulent mixing are smoothed, thanks to the k-l turbulent model. The lack of modeling for dense core striping, pseudo-atomization and dense cluster micro-mixing may be a factor for the discrepancies between the simulation and observations, particularly concerning the flame aperture angle. Nevertheless, the flame length is in good agreement with OH visualization (Figure 66).

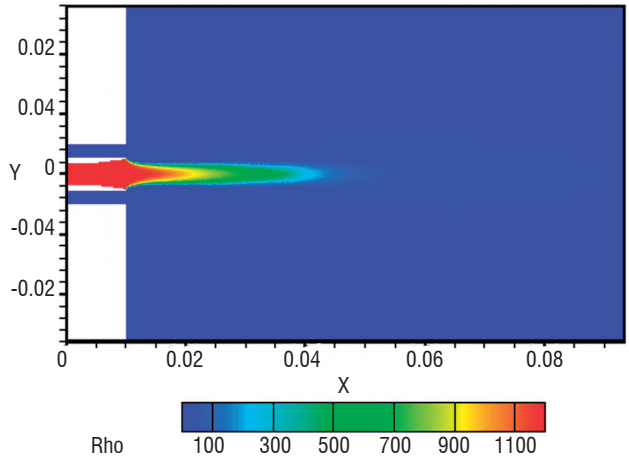

Figure 65 - Density field

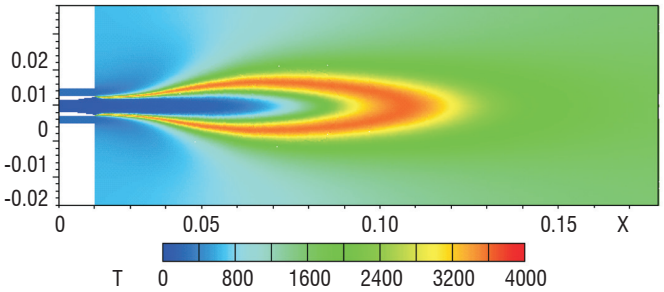

Figure 66 - Temperature field in the wake of the injector

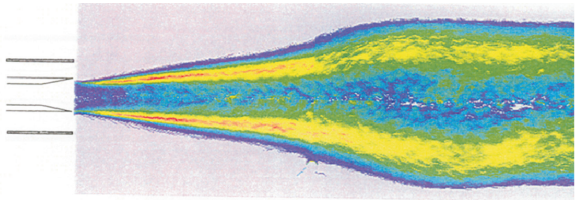

Figure 67 - OH emission visualization

Conclusion

Computation of a liquid rocket injector is one of the most difficult CFD challenges. In the subcritical case, an important issue is the primary atomization process, which would make it necessary to call upon a real two-fluid solver, able to describe the two phases and capture the interface instabilities: the development of this solver has been undertaken in CEDRE. In the supercritical case, the problem is topologically simpler, since the fluid can be considered as monophasic, but difficulty is reported in the thermodynamic modeling. The implementation of a real gas thermodynamic mo-

del in CEDRE allows us to perform successful computations in supercritical conditions. Besides the modeling improvement, the next step will be the extension of these computations to the LES approach.

Conclusion

The CEDRE code has been successfully used for many energetics or aerodynamics applications in the aerospace field. The main characteristics of the code (general unstructured mesh, general thermodynamics, multi-solver approach, explicit/implicit time integration, RANS/LES modeling, parallelization) are fully operational and many physical models are available for turbulence, combustion, atomization and radiation. The prediction accuracy level is very good for some cases, but remains perfectible for others, such as flow instabilities, pollutant emissions or two-phase flows. Future progress is expected from five main development axes:

- continuous improvement of physical modeling, especially for the RANS approach, including specific validations;
- generalization of the LES approach, allowed by the continuous increase of computing power;
- high order space discretization for unstructured grids;
- new solvers for general (non-dispersed) two-phase flows, namely a film solver and a seven-equation multifluid solver;
- generalization of the external coupling ■

References

[1] *CFD General Notation System/Standard Interface Data Structures*. AIAA Recommended Practice, R-101-200

[2] B. AUPOIX, D. ARNAL, H. BÉZARD, B. CHAOUAT, F. CHEDEVERGNE, S. DECK, V. GLEIZE, P. GRENARD and E. LAROCHE - T*ransition and Turbulence Modeling.* Aerospace Lab, Issue 2, March 2011

[3] A. BIANCHERIN, N. LUPOGLAZOFF, G. RAHIER and F. VUILLOT - *Comprehensive 3D Unsteady Simulations of Subsonic and Supersonic Hot Jet Flow-Fields.* Part 2: acoustic analysis, AIAA 2002-2600, 8th AIAA/CEAS Aeroacoustics Conference & Exhibit, June 17-19 2002, Breckenridge, CO

[4] G. BODARD, C. BAILLY and F. VUILLOT - *Matched Hybrid Approaches to Predict Jet Noise by Using Large-Eddy Simulation*. AIAA 2009-3316, 15th AIAA/CEAS Aeroacoustics Conference, 11 - 13 May 2009, Miami, Florida, USA

[5] C. BOGEY and C. BAILLY - *A family of Low Dissipative and Low Dispersive Explicit Schemes for Flow and Noise Computations.* Journal of Computational Physics, 194, 194-214, 2004

[6] C. BOGEY, S. BARRÉ, D. JUVÉ and C. BAILLY - *Simulation of a Hot Coaxial Jet : Direct Noise Prediction and Flow-Acoustics Correlations.* Phys. Fluids, Vol. 21, No. 3, 2009

[7] Y. BOURGAULT, W.G. HABASHI, J. DOMPIERRE and G.B. BARUZZI - *A Finite Element Method Study of Eulerian Droplets Impingement Models.* Int, Journal for Numerical Methods in Fluids, 1999

[8] L. CAMBIER and J.P. VEUILLOT - *Status of the elsA CFD Software for Flow Simulation and Multidisciplinary Applications.* AIAA-2008-0664, 46th AIAA Aerospace Sciences Meeting, Reno, NV, 2008

[9] J.T. CANSDALE and I.I. MCNAUGHTAN - *Calculation of Surface Temperature and Ice Accretion Rate in a Mixed Water Droplet/ice Crystal Cloud.* Royal Aircraft Establishment Technical Report. 77090, 1977

[10] F. CHEDEVERGNE - *Advanced Wall Model for Aerothermodynamics.* International Journal of Heat and Fluid Flows, accepted

[11] S. CHEMIN - *Etude des interactions fluide/structure par un couplage de codes de calcul*. Ph.D. Thesis, Université de Reims Champagne-Ardennes, 2006

[12] B. COURBET, C. BENOIT, V. COUAILLIER, F. HAIDER, M.C. LE PAPE and S. PÉRON - *Space Discretization Methods*. Aerospace Lab, Issue 2, March 2011

[13] W. DODDS - *Engine and Aircraft Technologies to Reduce Emissions.* UC Technology Transfer Symposium « Dreams of Flights », San Diego, March 2002

[14] F. DUPOIRIEUX and N. BERTIER - *The models of Turbulent Combustion in the CHARME solver of CEDRE*. Aerospace Lab, Issue 2, March 2011

[15] D. DUTOYA and L. MATUSZEWSKI - *Thermodynamics in CEDRE*. Aerospace Lab, Issue 2, March 2011

[16] D.R. EKLUND, J.P. DRUMMOND and H.A. HASSAN - *Calculation of Supersonic Turbulent Reacting Coaxial Jets.* AIAA Journal 28 (9), pp. 1633-1641, 1990

[17] M.P. ERRERA and S. CHEMIN - *A Fluid-Solid Thermal Coupling Applied to an Effusion Cooling System*. 34th AIAA Fluid Dynamics Conference and Exhibit, AIAA Paper 2004-2140, Portland, 28 June-1st July 2004

[18] M.P. ERRERA, A. DUGEAI, P. GIRODROUX-LAVIGNE, J.D. GARAUD, M. POINOT, S. CERQUEIRA and G. CHAINERAY - *Multi-Physics Coupling Approaches for Aerospace Numerical Simulations.* Aerospace Lab, Issue 2, March 2011

[19] F. FALEMPIN and L. SERRE - *LEA Flight Test Program – A First Step to an Operational Application of High-Speed Air Breathing Propulsion*. AIAA 2003-7031, Norfolk

[20] F. FALEMPIN and L. SERRE - *French Flight Testing Program LEA* – Status in 2009, AIAA 2009-7227, Bremen

[21] M.B. GILES - *Stability Analysis of Numerical Interface Conditions in Fluid-Structure Thermal Analysis.* International Journal for Numerical Methods in Fluids, Vol. 25, 1997, pp 421-436

[22] F. GUILLOU - F. CHEDEVERGNE - *Internal Turbine Blade Cooling Simulation : the Smooth BATHIRE Rig Configuration*. ERCOFTAC ETMM8 2010, Marseille, France

[23] M. HABIBALLAH, L. VINGERT, J.C. TRAINEAU and P. VUILLERMOZ - MASCOTTE : *A Test Bench for Cryogenic Combustion Research*. 47th International Astronautical Congress, Beijing (China), October 7-11, 1996

[24] A. HADJADJ and M. ONOFRI - *Nozzle Flow Separation.* Shock Waves, 19 :163–169, 2009

[25] M. HUET, B. FAYARD, G. RAHIER and F. VUILLOT - *Numerical Investigation of the Micro-Jets Efficiency for Jet Noise Reduction*. AIAA-2009-3127, 15th AIAA/CEAS Aeroacoustics Conference, 11 - 13 May 2009, Miami, Florida, USA

[26] M. HUET, F. VUILLOT and G.RAHIER - *Numerical Study of the Influence of Temperature and Micro-Jets on Subsonic Jet Noise*. 14th AIAA/CEAS, Aeroacoustics Conference, Vancouver, Canada, 2008

[27] E. LAROCHE - *Influence of Freestream Turbulence Intensity on Cooling Effectiveness*. ASME PAPER 2001-GT-0139

[28] N. LUPOGLAZOFF, G. RAHIER and F. VUILLOT - *Application of the Cedre Unstructured Flow Solver to Jet Noise Computations*. 1st EUCASS, 4-7 July 2005, Moscow

[29] B. F. MAGNUSSEN and B.H. HJERTAGER - *On Mathematical Models of Turbulent Combustion With Special Emphasis on Soot Formation and Combustion*. 16th Symposium (International) on Combustion, pp. 719-729, Pittsburgh, 1977

[30] H. MENG and V. YANG - *A unified Treatment of General Fluid Thermodynamics and its Application to a Preconditioning Scheme*. Journal of Computational Physics 189 (2003), pp. 277-304

[31] B.L. MESSINGER - *Equilibrium Temperature of an Unheated Icing Surface as a Function of Air Speed.* Journal of the Aeronautical Sciences, Vol. 20, No. 1, pp. 29-42, 1953

[32] E. MONTREUIL, A. CHAZOTTES, D. GUFFOND, A. MURRONE, F. CAMINADE and S. CATRIS - *Enhancement of Prediction Capability in Icing Accretion and related Performance Penalties*. Part I: Three-dimensional CFD Prediction of the Ice accretion, The 1st Atmospheric and Space Environments, San Antonio, Texas, AIAA, 2009

[33] F. MULLER, F. VUILLOT, G. RAHIER and G. CASALIS - *Modal Analysis of a Subsonic Hot Jet LES with Comparison to the Linear Stability Analysis.* AIAA-2005-2886, 11th AIAA/CEAS Aeroacoustics Conference, 23-25 May 2005, Monterey, California, USA

[34] F. MULLER, F. VUILLOT, G. RAHIER, G. CASALIS and E. PIOT - *Experimental and Numerical Investigation of the Near Field Pressure of a High Subsonic Hot Jet*. AIAA-2006-2535, 12th AIAA/CEAS Aeroacoustics Conference, 8-10 May, 2006, Cambridge, MA, USA

[35] A. MURRONE and D. SCHERRER - *Large Eddy Simulation of a Turbulent Premixed Flame Stabilized by a Backward Facing Step*. 1st INCA Workshop, 2005, Villaroche (France)

[36] A. MURRONE and P. VILLEDIEU - *Numerical Modeling of Dispersed 2-Phase Flow*. Aerospace Lab, Issue 2, March 2011

[37] A. NICOLE, F. DUPOIRIEUX, L. VINGERT, M. HABIBALLAH and M. THERON - *Simulation of a Subcritical LOX/GH2 MASCOTTE Test Case (10 bar).* 5th International Spacecraft Propulsion Conference , 5-8 May 2008, Heraklion (Greece)

[38] G. ORDONNEAU, P. HERVAT, F. GRISCH, L. VINGERT and P. REIJASSE - *PLIF Investigation of Reactive Flows in the Separation Region of an Over-expanded Two-Dimensional Nozzle.* AIAA Paper, number 2006-5209, 2006

[39] M. PAPADAKIS, R. ELANGONAN, G.A. JR. FREUND, M. BREER, G.W. ZUMWALT and L. WHITMER - *An experimental Method for Measuring Water Droplet Impingement Efficiency on Two-and Three-Dimensional Bodies.* NASA CR 4257

[40] E. PIOT, G. CASALIS, F. MULLER and C. BAILLY - *Investigation of the PSE Approach for Subsonic and Supersonic Hot Jets. Detailed Comparisons With LES and Linearized Euler Equations Results.* Int. J. of Aeroacoustics, Vol. 5, No. 4, pp. 361 – 393, 2006

[41] M.G. POTAPCZUK and C.S. BIDWELL - *Numerical Simulation of Ice Growth on a MS-317 Swept Wing Geometry*. AIAA-91-0263, 39th Aerospace Sciences Meeting, Reno, NV, 1991

[42] G. RAHIER, J. PRIEUR, F. VUILLOT, N. LUPOGLAZOFF and A. BIANCHERIN - *Investigation of Integral Surface Formulations for Acoustic Post-Processing of Unsteady Aerodynamic Jet Simulations*. Aerospace Science and Technology, Vol. 8, pp. 453-467, 2004

[43] A. REFLOCH, B. COURBET, G. CHAINERAY, J.B. DARGAUD, P. GILBANK, C. LAURENT, A. MURRONE, E. QUÉMERAIS, L. TESSÉ, J. TROYES, F. VUILLOT and P. VILLEDIEU - *CEDRE Software*. Aerospace Lab, Issue 2, March 2011

[44] S. REICHSTADT - *Etude du mélange et de la combustion monophasique dans un statoréacteur de recherche.* Ph.D. Thesis, Université de Pau et des Pays de l'Adour, 2007

[45] S. REICHSTADT, N. BERTIER, A. RISTORI and P. BRUEL - *Towards LES of Mixing Processes Inside a Research Ramjet Combustor*. 18th International Society of Air Breathing Engines (ISABE), Beijing, China, 2007

[46] G. RIBERT, N. ZONG, V. YANG, L.PONS, N. DARABIHA and S. CANDEL - *Counterflow Diffusion Flames of General Fluids: Oxygen/Hydrogen Mixtures.* Combustion and Flame 154, pp. 319-330, 2008

[47] A. RISTORI, G. HEID, C.BROSSARD and A. BRESSON - *Characterization of the Reacting Two-Phase Flow Inside a Research Ramjet Combustor.* International Conference on Liquid Atomization And Spray Systems ICLASS'03, Sorrento, Italy, 2003

[48] A. RISTORI, S. REICHSTADT, C.BROSSARD and G. HEID - *PIV and Gas Sampling Analysis Measurements for Fuel-to-Air Mixing Study Inside a Research Ramjet Combustor.* 13th International Symposium on Flow Visualization ISFV13 / 12th French Congress on Visualization in Fluid Mechanics FLUVISU12, Nice, France (2008)

[49] A. RISTORI, Y. SERVOUZE, M. BARAT and F. SOULIGNAC - *PIV Flow Characterization Inside a Large-Scale U-Shaped Rotating Channel.* Onera-DLR Aerospace Symposium, Göttingen, Germany

[50] B. SAINTE-ROSE, N. BERTIER, S. DECK and F. DUPOIRIEUX - *A DES Method Applied to a Backward Facing Step Reactive Flow*. C. R. Mec., 337 (6-7): 340–351, 2009

[51] L. SERRE and F. FALEMPIN - PROMETHEE : *the French Military Hypersonic Propulsion program.* Status in 2002, AIAA 2003-6950, Norfolk

[52] M. SHUR, P. SPALART and M. STRELETS - *Noise Prediction for Increasingly Complex Jets*. Part I: Methods and Tests. Part II: Applications, Int. J. Aeroacoustics, Vol. 4, No. 3+4, pp. 213-266, 2005

[53] D. L. STRAUB, K. H. CASLETON, R. E. LEWIS, T. G. SIDWELL, D. J. MALONEY and G. A. RICHARDS - *Assessment of Rich-Burn, Quick-Mix, Lean-Burn Trapped Vortex Combustor for Stationary Gas Turbine*. Journal of engineering for gas turbine and power, 27 :36-41, 2005

[54] M. TELARA, L. JACQUES, P. LE HELLEY, T. PEVERGNE and D. RIBEREAU - *A New Concept to Reduce SRM Pressure Oscillations: the 3D Frontal Thermal Protection*. European Conference in Aerospace Sciences (EUCASS), 2005

[55] L. TESSÉ and J.M. LAMET - *Radiative Transfer Modeling Developed at Onera for Numerical Simulation of Reactive Flows*. Aerospace Lab, Issue 2, March 2011

[56] J. TROYES and F. VUILLOT - *Numerical Simulations of a Model solid Rocket Motor Ignition Overpressure Wave*. 44th AIAA/ASME/SAE/ASEE JPC, 2008

[57] J. TROYES, F. VUILLOT, J. VARNIER and P. MALBÉQUI - *Numerical Simulations of Rocket Solid Motor Engine Ignition and Duct Overpressure Waves at Reduced Scale.* 45th AIAA/ASME/SAE/ASEE JPC, 2009

[58] J. VARNIER, P. PRÉVOT, G. DUNET, M. BARAT and B. BAZIN - *Blast Wave and Afterburning at Ignition of Rocket Engines*. 13th ICSV, 2006

[59] K. VISWANATHAN, M. SHUR, P. SPALART and M. STRELETS - *Flow and Noise Predictions for Single and Dual-Stream Beveled Nozzles*. AIAA Journal, Vol. 46, No. 3, pp. 601-626, March 2008

[60] F. VUILLOT, N. LUPOGLAZOFF and M. HUET - *Effect of a Pylon on Double Stream Jet Noise from Hybrid CAA Computations*. AIAA-2010-2049, 16th AIAA/CEAS Aeroacoustics Conference, 7-9 June 2010, Stockholm, Sweden

[61] F. VUILLOT, N. LUPOGLAZOFF and G. RAHIER - *Double-Stream Nozzles Flow and Noise Computations and Comparisons to Experiments*. AIAA-2008-0009, 46th AIAA Aerospace Sciences Meeting and Exhibit, 7-10 Jan. 2008, Reno, NV, USA

[62] S. WALLIN and A.V. JOHANSSON - *An Explicit Algebraic Reynolds Stress Model for Incompressible and Compressible Turbulent Flows*. Journal of fluid mechanics, Vol. 403, pp 89-102

[63] P.M. WIKSTRÖM, S. WALLIN and A.V. JOHANSSON - *Derivation and Investigation of a New Explicit Algebraic Model for Passive Scalar Flux*. Physics of Fluids, Vol. 12, pp 688-702.

[64] B. ZAMUNER and F. DUPOIRIEUX - *Numerical Simulation of Soot Formation in a Turbulent Flame With a Monte-Carlo PDF Approach and Detailed Chemistry*. CST, 158 :407-438, 2000

Acronyms:

AEID (Acoustique et Environnement Induit au Décollage)
AUSM (Advection Upstream Splitting Method)
CAA (Computational Aero-Acoustics)
CARS (Coherent Anti-Stokes Raman Scattering)
CFD (Computational Fluid Dynamics)
CGNS (CFD General Notation System)
CPU (Central Processing Unit)
CNES (Centre National d'Etudes Spatiales)
DDES (Delayed Detached Eddy Simulation)
DNS (Direct Numerical Simulation)
DOM (Discrete Ordinates Method)
DOP (Duct Over Pressure)
EAHFM (Explicit Algebraic Heat Flux Model)
EARSM (Eplicit Algebraic Reynolds Stress Model)
EBU (Eddy-Break-Up)
EVM (Extended Vullis Model)
GMRES (Generalized Minimal RESidual)
IOP (Ignition Over Pressure)
LEA (Liotnii Experimentalnii Apparat)
LES (Large Eddy Simulation)
LFRJ (Liquid Fueled RamJet)
MILES (Monotone Integrated Large-Eddy Simulation)
MUSCL (Monotone Upstream Schemes for Conservation Laws)
OVS (Obstacle Vortex Shedding)
PDF (Probability Density Function)
PIV (Particle Image Velocimetry)
PLIF (Planar Laser Induced Fluorescence)
PVS (Parietal Vortex Shedding)
RANS (Reynolds Averaged Navier-Stokes)
RMS (Root Mean Square)
SDR (Solid Ducted Rocket)
SIBLE (Simple Integrated Boundary Layer Equations)
SRM (Solid Rocket Motor)
SST (Shear Stress Transport)
TAPS (Twin Annular Premixing Swirling)
TPaSR (Transported Partially Stirred Reactor)

Dominique Scherrer graduated from «Ecole Centrale de Paris» in 1979. He joined Onera in the Energetics Direction in 1981. His main research topics concerned droplet combustion modeling, combined cycle propulsion, scramjet design and CFD. He has been the CEDRE project manager between 1996 and 2002. He is deputy director of the Fundamental and Applied Energetics Department since 1997.

François Chedevergne graduated from a french engineer school (Supaéro), Dr. François Chedevergne is a research scientist working at Onera within the Fundamental and Applied Energetics Department. He is in charge of the aerothermodynamics studies of the department and is deeply involved in the development of the software platform CEDRE regarding turbulence modelling.

Philippe Grenard graduated from the french engineer school École Polytechnique and Sup'Aéro in 2004. He is a research engineer working at Onera in the Fundamental and Applied Energetics Departement (DEFA). He is in charge of computational activities regarding the in-house CEDRE platform (modelling, development and computations) in the Liquid Propulsion Unit. His activities focus on combustion and thermal loads in the combustion chamber and nozzle of liquid propellant engines.

Julien Troyes received a Master Degree in «Modelisation and Simulation in Mechanics» in 1999 at Joseph Fourier University in Grenoble, France. He has been working at Onera as a research engineer since november 2000. His main activity is dedicated to the validation of the CEDRE software. Apart from this general topics, his research activities are focused on solid rocket motor jet applications (infrared signatures, ignition and duct overpressures waves ...).

Angelo Murrone graduated from "Institut Universitaire des Systèmes Thermiques Industriels " in 2000 and received his Ph. D. Degree in Mechanics and Energetics from "Université de Provence Aix-Marseille I" in 2003. He has been working as a research scientist in the Fundamental and Applied Energetics Department at Onera since 2004. His research concerns the numerical modeling of "dispersed" and "separated" two-phase flows. He is currently in charge of the development of the Eulerian solver SPIREE in the CEDRE code.

Emmanuel Montreuil (Associate Professor) obtained his Ph. D. Degree in Mechanics from "Université Pierre et Marie Curie – Paris 6" in 2000. He joined Onera in 2002 and has been involved in aircraft and rotorcraft icing for over 8 years, working on projects funding by the French civil aviation. He has been involved in both the development and application of several icing codes (2D and 3D), and has taken part in icing wind tunnel test campaigns in the frame work of the Onera-NASA-UIUC collaboration. He has organised and chaired sessions for the AIAA.

François Vuillot head of the 'software design and integration for the multi-physics and energetics unit at Onera, in charge of CEDRE software.

Nicolas Lupoglazoff graduated from « Ecole Nationale Supérieure de l'Aéronautique et de l'Espace» in 1987. He joined Onera in 1989 at the Energetics Direction. He is working in the CFD field and is specialized in aerodynamics and acoustics in engines, nozzles and jets.

Maxime Huet graduated from the "Ecole Centrale de Lyon" in 2006 and received a Master degree in Acoustics from Lyon University the same year. He joined Onera in 2007 as a research scientist. His work is mainly dedicated to jet and combustion noise simulations and their possible reduction.

Bruno Sainte-Rose graduated from "Ecole Centrale de Paris" in 2006 and received his Ph. D. Degree in Energetics in 2010. His Ph. D. thesis was focused on the development of turbulence and combustion models in Onera's code CEDRE. The aim of this work was to be able to run unsteady simulations of separated reactive flows. He joined the LEMMA company (Houston, Texas) in 2010, where he is working as a project engineer.

Pascal Thorigny joined Onera in 2001 after being graduated from ESTACA (Ecole Supérieure des Techniques Aéronautiques et de Construction Automobile). He is working in the Applied Aerodynamics Department in the "Missiles, Hypersonic and Launchers" unit as a CFD and mesh generation expert engineer. He his responsible for store separation under combat aircraft studies and in charge of the external aerodynamics and the booster separation phase characterisations of hypersonic vehicles like in the LEA project.

Nicolas Bertier graduated from ENS Cachan and PhD from Paris VI University (2006), is senior researcher in the Energetics department of Onera. He is in charge of the numerical simulation of reactive flows in aeronautic combustors. He has developed and validated the numerical methods and combustion models that were required to carry out LES with the CEDRE code of Onera. He is also teaching "energetics of aeronautic combustors" at Paris VI University.

Jean-Michel Lamet graduated from the « École Superieure d'Ingénieurs de Poitiers » in 2005 and received his Ph.D. degree from « École Centrale de Paris » in 2009. During his Ph.D., he worked on the radiative transfer in atmospheric re-entry hypersonic flows. He now holds a position of research scientist in the Applied and Fundamental Energetic Department of Onera. His activity includes modelling and simulation of radiative transfer in combustion chambers and hypersonic flows. He is involved in the development of the ASTRE and REA code dedicated to radiative transfer.

Thomas Le Pichon graduated from ENSMA in 2008. He has been responsible for the Research Ramjet Program since 2009. This activity includes experimental and numerical study of the reacting flow in the Research Ramjet combustion chamber. His recent activities focused on combustion efficiency prediction, combustion instabilities and lean blow-out phenomenon.

Emmanuel Radenac is a research scientist at Onera. He graduated in 2003 from « Ecole Nationale Supérieure de l'Aéronautique et de l'Espace » and received his Ph.D. degree in 2006. During his Ph.D., he worked on numerical methods for thermal coupling of fluid and solid solvers (CHARME and ACACIA for CEDRE). Since 2007, he has been working in the field of solid propulsion.

Aurélie Nicole graduated in 1997 from ENSEEIHT in Toulouse. Then she completed her Fluid Mechanics Engineering Degree by 18 months of research at the University of Kyoto (Japan) in the nuclear engineering department. After having worked one year in the department of future project at CNES, she joined Onera in 2000 and started working on liquid rocket combustion instability. Since her arrival, she is in charged of the researches on high frequency instabilities and of the numerical simulation of reacting flow in liquid propulsion.

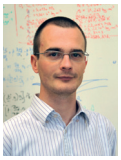

Lionel Matuszewski is a research engineer at the Onera working in the Liquid Propulsion Unit of the Fundamental and Applied Energetics Department (DEFA). He graduated from the Ecole Polytechnique and ISAE engineer schools in 2007. His research field is mainly focused on dense fluid modeling with application to supercritical combustion.

Marc Errera graduated from the "Ecole Centrale de Paris" in 1980 and obtained a Research Habilitation Thesis (Thèse d'Etat) from the University Pierre & Marie Curie (Paris 6) in 1990, in the field of in-cylinder flow in reciprocating engines. He is currently in charge of multidisciplinary projects.